OPTIMUM PREFORM AND DIE SHAPE DESIGN FOR IMPROVED HARDNESS DISTRIBUTION IN COLD FORGED PARTS

by

Haluk Tümer

B.S., in Mechanical Engineering, Istanbul Technical University, 2004

Submitted to the Institute for Graduate Studies in
Science and Engineering in partial fulfillment of
the requirements for the degree of
Master of Science

Graduate Program in Mechanical Engineering
Boğaziçi University

2007

ACKNOWLEDGEMENTS

I would like to thank my advisor Assoc. Prof. Fazıl Önder Sönmez for his guidance and continuous support during the preparation of this thesis.

I would like to express my gratitude to the assistants and colleagues at the Department of the Mechanical Engineereing of Boğaziçi University, especially Ahmet H. Ertaş, for his support and motivation.

Finally, I would like to thank my family for their support, patience and encouragements.

ABSTRACT

OPTIMUM DIE AND PREFORM SHAPE DESIGN FOR IMPROVED HARDNESS DISTRIBUTION IN COLD FORGED PARTS

To predict and then to control hardness distribution in a cold formed part is important, since it is a critical property due to its effects on the forgability of the part and its performance in use.

In cold forming processes, hardness of the workpiece is increased as a result of work hardening. The amount of increase is related to the extent of induced plastic strains. This strain-hardness relation may be expressed analytically. Thus, one may obtain the hardness distribution in a cold formed part, once the material properties and induced plastic strains are known.

In this research, a methodology is proposed to improve the hardness distribution in a backward extruded cup by optimizing die and preform shapes. Firstly, a finite element model of the backward extrusion process was developed to obtain the effective strain distribution. Then, an analytical relation between strain and hardness was used to determine the hardness distribution. Two variables defining the punch tip geometry and one variable defining the die were selected as optimization variables. The ranges of values that optimization variables could take were constrained. Nelder-Mead was used as the search algorithm to find the optimum process design. An optimization code was developed incorporating the finite element model and the optimization procedure.

The results show that significant improvements in hardness distribution can be achieved using the proposed optimization procedure. It was found that the smaller the die clearance, the more uniform the hardness distribution would be. Moreover, it was observed that a smaller friction constant for die-workpiece interface results in a more homogenized hardness distribution.

ÖZET

SOĞUK DÖVME PARÇALARDA SERTLİK DAĞILIMININ KALIP VE İŞ PARÇASI BAŞLANGIÇ ŞEKİLLERİNİN OPTİMİZASYONU YOLUYLA İYİLEŞTİRİLMESİ

Soğuk şekilendirme yöntemleriyle ile imal edilmiş parçalarda sertlik dağılımı, parçanın şekillendirilebilirliğine ve kullanım sürecindeki performansına olan etkisi nedeniyle önem taşır.

Soğuk şekillendirme uygulamalarında iş parçasının sertliği pekleşme sonucu artar. Bu artış, uygulanan plastik şekil değiştirme miktarı ile ilişkilidir. Bu ilişki analitik olarak ifade edilebilir. Bu ilişkinin, ilgili malzeme özelliklerinin ve meydana gelen plastik şekil değişimlerinin bilinmesi halinde, iş parçasındaki sertlik dağılımı bulunabilir.

Bu çalışmada, geri ekstrüzyon yöntemi ile imal edilmiş parçada, kalıp ve iş parçası başlangıç geometrilerinin optimizasyonuyla, sertlik dağılımının iyileştirilmesi amacına yönelik yöntem geliştirilmiştir. Meydana gelen plastik şekil değişiminin bulunması amacıyla, işlemin sonlu elemen modeli hazırlanmıştır. Ardından sertlik ve şekil değişimi arasındaki analitik ilişkiden faydalanılarak sertlik dağılımı elde edilmiştir. Bunu takiben kalıp geometrisini tanımlayan iki ve kalıp boşluğunu belirleyen bir optimizasyon değişkeni tanımlanmıştır. Bu değişkenlerin alabileceği değerler için sınırlar tanımlanmıştır. Son adımda, Nelder-Mead yöntemini baz alan optimizasyon kodu hazırlanmış, hazırlanan bu kod sonlu elemanlar modeliyle ilişkilendirilmiştir.

Sonuç olarak, sertlik dağılımınında önemli derecede iyileşme sağlanmıştır. Ek olarak, kalıp ve iş parçası arasında sürtünme katsayısının en aza indirilmesinin, sertlikte daha az değişimi beraberinde getirdiği görülmüştür. Ayrıca, kalıp boşluğunda azalmanın sertlik değişiminin azaltılması yönünde olumlu etkisi olduğu gözlenmiştir.

TABLE OF CONTENTS

LIST OF FIGURES

LIST OF TABLES

LIST OF SYMBOLS

A	Projected area of the pyramidal indentation
a	contact length of the pyramidal indentation
Dw	Diameter of the workpiece
e	Engineering strain
e_1	First principle plastic strain
e_2	Second principle plastic strain
e_3	Third principle plastic strain
f	Value of the objective function
F	Applied load in Vickers hardness test
h	Depth of the pyramidal indentation
HV	Vickers hardness
HV_{avg}	Avarage Vickers hardness
HV_i	Vickers hardness value of the node i
HVE_i	Vickers hardness error of the node i
HVE_T	Total Vickers hardness error
K	Strength coefficient
k	Number of design variables
$L1$	Length of the workpiece
m	Friction factor
n	Strain hardening coefficient
P_a	Analysis penalty
P_k	Constraint penalty
P_m	Mean pressure applied in Vickers hardness test
$R1$	Radius of the spherical punch tip
$R2$	Corner radius of the spherical punch tip
s	Length of the base diagonal of the pyramidal indentation
t	Die clearance
w_1	Weighting factor of the constraint penalties
w_2	Weigthting factor of the analysis penalty

ε_o	Effective strain
ε_e	Representative strain
ε	True strain
σ_e	Representative stress
σ	True stress
η	Control term of the analysis penalty

1. INTRODUCTION

In the last decades, cold forging has become one of the most widely used production methods due to its various advantages. Firstly, cold forming helps not only to produce parts of superior mechanical properties with better dimensional accuracy and surface finish, but also minimizes material waste compared to material removal processes. Moreover, forging to net or near net shape dimensions reduces the need for post processes, resulting in significant cost savings. On the other hand, since the tooling and equipment costs are relatively high, the process is feasible when parts are to be produced in large numbers in order to remain competitive. [1]

Process parameters like preform geometry, the number of stages through which the process is achieved and heat treatments in each of them, significantly affect the success of the process with regard to product quality and cost. In order to decrease manufacturing costs and ensure the quality of the product, the process designers should be able to predict correctly the effects of process parameters on the geometric and mechanical properties of the finished product. If the process is not properly designed, costly changes have to be made in tooling and equipment. In other words, the ever- increasing competition forces the manufacturers to decrease product development times and increase the quality of the end product, which require that forging process and tooling be designed with minimum effort spent on trial and error.

In applications demanding high hardness levels usually expensive high carbon-high alloy steels are chosen. Low carbon and low alloy steels are not ideal for heat treatment processes compared to high alloy-high carbon steels. Firstly, they may need additional processes like carburizing to achieve desired hardness level and depth. Secondly, heat treated parts may fail due to crack development and excessive distortions. On the other hand, increased hardness of the cold forged parts may allow the use of low carbon steels in applications where high hardness is required. This means that instead of expensive alloy steels, use of cheap low carbon steels decreases the material cost as well as the cost of heat treatment.

In cold forging operations, hardness is not only an output of the process and a quality parameter of the end product, but it is also a parameter, which must also be monitored during the process. During cold forging of a part, the material might become so hard that the available press power may become unable to deform the workpiece further or the dies and the part itself might be damaged. In order to overcome this problem, forging operations are usually completed in sub-steps followed by annealing. A cold forming process should therefore be carefully designed so that hardness of the material during as well as after the processing remains within the acceptable limits. The methods explained in this thesis can be used to predict the hardening effect and determine the required cold forging sub-steps, although the hardness of the finished part is our main concern in this study.

Hardness is an important quality parameter considering that it is a measure of strength and resistance to wear so it highly influences the performance of products in the service life. High levels of hardness in a finished product may increase its performance for instance in metal cutting applications but its accompanying low toughness makes this part unsuitable for applications requiring high impacts resistance. Uneven hardness distribution is another concern. The regions of high hardness may make the part brittle while the regions of low hardness may detract from its wear resistance, therefore making the part unsuitable for both types of applications requiring either high hardness or high toughness. In this study, a method is proposed for optimal process design that makes use of finite element analysis, computer aided design and optimization techniques. The aim is to control the resulting hardness distribution by optimizing preform and die geometry.

Permanent deformation induced during cold forming leads to increased hardness. By controlling deformations in a cold forging process, one may control and thus achieve a desired level of hardness. Two of the most important factors affecting deformations are shapes of preform and die. In order to control hardness through deformation, one should know the relationship between deformation and hardness in a cold forged part. One may relate process parameters to deformation through finite element modeling of the process. Once the controllable process parameters are related to hardness, one may control hardness. Then, one may find the set of process parameters resulting in the desired hardness distribution through an optimization procedure.

In the literature, there were a number of studies on optimization of cold forging processes. Most of them focused on two major objectives. The first one was to obtain an accurate final geometry and the second one was to decrease the applied pressure in order to lower the required press capacity, and thus to prevent dies from failures and improve tooling life. On the other hand, there were also optimization studies having different objectives such as improving microstructural properties.

The objective of Thiyagarajan and Grandhi's study [2] was to reduce the difference between the desired and achieved geometries of the finished product (die underfill) and to minimize the strain variance by optimizing basis shapes in multi-level forging processes. They defined the boundary curves of basis shapes by means of coordinates of control points lying on these boundary curves (Figure 1.1). They applied the reduced basis technique to decrease the number of optimization variables. Thiyagarajan and Grandhi selected response surface methodology (RSM) to build approximation model and perform optimization. The proposed model was applied on multi-level forging of a steering link. They reported that a preform shape that enables complete die fill was achieved in two levels.

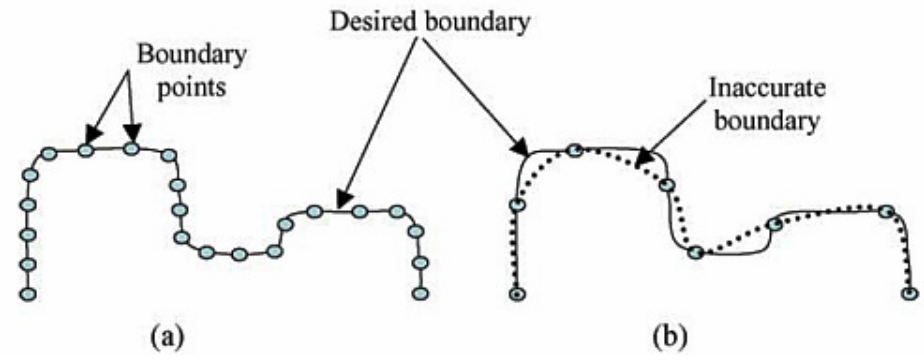

Figure 1.1. Definition of basis shapes (a) and die underfill (b) [2]

Zhao and Wang [3] proposed an optimization method for preform shape design. The objective was to minimize the effective strain variation in an H-shaped forging. They defined the preform die shape through B-spline curves. The coordinates of control points were design variables. In 2D case, for n control points there were $2n$ design variables (x, y coordinates of each point). The objective function was given in Eq. **Error! Reference source not found.**, where ε_i is the effective strain in the i^{th} element where ε_{av} is the average effective strain in the part. N is the total number of elements, and

V_i is the weighting factor for the i^{th} element depending on the area occupied by this element. Broyden-Fletcher-Goldfarb-Shanno (BFGS) algorithm was employed to minimize the objective function. The final maximum and minimum strains were obtained to be 1.3608 and 0.35, respectively; they were 1.6053 and 0.2961 for the non-optimized case.

$$\psi = \sum_{i=1}^{N} \frac{V_i(\varepsilon_i - \varepsilon_{av})}{N} \tag{1.1}$$

Although there are similarities between Zhao and Wang's study and the present study, e.g. FEM is employed to obtain effective strains; our objective is to obtain a uniform hardness distribution in a cold forged part, which is directly related to the part quality, rather than to minimize the variation in effective strain.

Shi *et al*. [4] proposed a shape optimization technique to improve stamping quality by minimizing the risk of rapture, wrinkles and unstretched areas. Selected optimization variables were shape perturbation vectors on addendum surface and draw bead height on binder surfaces. They utilized Modified Sweeping Simplex as a search algorithm. They integrated this algorithm with FE modeling and applied this on a front fender for validation of results.

Celano *et al*. [5] developed a technique for optimum process design of multi-pass cold drawing process using Simulated Annealing. The objective of this study was to determine optimum number of passes and pass-schedule to keep in wire developed stresses below a safety limit. They also showed the effectiveness of their approach by comparing it with a set of industrial sequences for wires of different materials.

Gao and Grandhi [6] proposed a sensitivity analysis based optimization method for improving the grain size variation in forged parts. The optimization variables were billet shape and die velocity. They also set optimization constraints for die underfill and excessive material waste. They applied their method on a turbine disk of waspaloy (a nickel base, age-hardenable superalloy) and obtained optimum billet geometry and die velocity.

Roy *et al*. [7] carried out a comprehensive study on optimization of multi-stage cold forming processes. Multi-pass cold wire drawing, multi-pass cold tubular profile drawing and multi-pass cold forging of an automotive outer race were the selected processes. They used a micro genetic algorithm to optimize the process variables. In case of multi pass-cold wire drawing, die approach angles, the area reduction ratio and the number of passes were optimization variables. The two objective functions to be minimized were the difference between the maximum and minimum the effective plastic strains and the total deformation energy. Consequently, they managed to drop the number of passes from six to four, and the difference between the extremum effective plastic strains was remarkably lower. In optimization of multi-pass cold tubular profile drawing, the related optimization variables were the inner and outer diameters of the circular tubular profile and the die length. In this case, the objective was minimization of underfill. Lastly, they worked on optimization of cold forging of an automotive outer race consisting of three sub-steps (one extrusion and one upsetting). A schematic of the process is given in Figure 1.2. The optimization variables in the extrusion sub-step were radius of the initial billet, the angle of extrusion and the length of the extrude, whereas the optimization variables were guide length, half cone angle and the gap between the top and bottom die for upsetting sub-steps. The objective function for this case was the damage value defined as an integrated value based on a ductile fracture criterion. The optimization resulted in a 42 per cent reduction in damage value. The study of Roy *et al*. showed the effectiveness of optimization in cold forging processes as well as the effectiveness of the micro genetic algorithm.

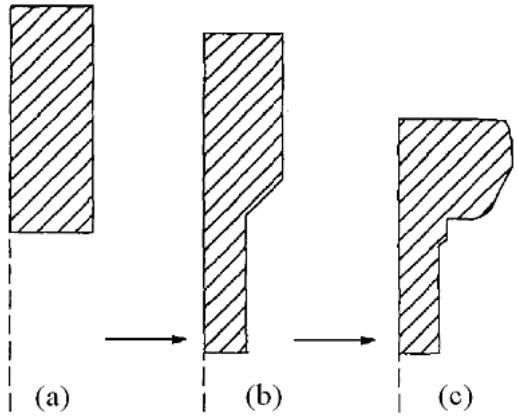

Figure 1.2. Starting material (a), as extruded (b) and up set [7]

The literature survey shows that there has been no study on controlling the hardness of cold forged parts by optimizing geometries of preform and die. In this study, a methodology for optimum process design of cold formed parts was proposed to obtain uniform hardness distribution. Backward extrusion was chosen as the process type to be optimized. First, a finite element model of the process was developed in ANSYS environment. This FE model enabled calculation of induced effective strains in the part. Then, the strain-hardness relationship proposed by Sönmez and Demir [8] was used to convert effective strain values to hardness and thus to determine the hardness distribution. The next step was to develop an optimization code based on Nelder-Mead algorithm. The objective was defined as the sum of variations from the average hardness in the part, and some of the geometric parameters defining die and preform shapes were chosen as optimization variables. At last, the FE model and the optimization code were integrated. Having carried out optimization, optimum preform and die shapes were determined.

2. PROBLEM STATEMENT

The aim of this study is to optimize die and workpiece geometry to minimize variation of hardness distribution in a cold forged product. The type of the cold forging process in concern is backward (cup) extrusion. This process is selected because of its prevalence in the industry, higher variation in the strain distribution as a result of large strains induced in the workpiece and compatibility to axisymmetric modeling, which decreases computational cost.

The geometries of the die and workpiece are depicted in Figure 2.1, while the geometry of the part to be extruded backward is shown in Figure 2.2. The geometries described in these figures were adopted from the study of Hur *et al*. [9] in which a design method for FE analysis of backward extrusion process was proposed. The thickness of the walls, the height and depth of the cup are assumed to be specified according to the requirements of the product. In backward extrusion, the punch tip is not chosen to be flat to decrease the press capacity required for inducing the desired deformations. Thus, the punch tip is to be curved. The radii of curvatures, *R1* and *R2,* defining the tip geometry of the punch are assumed to be variables that can be determined during the process design phase. Only, upper and lower limits may be set because of the requirements of the product during the product design phase. The initial shape of the workpiece is cylindrical. A gap exists between the preform and the inside walls of the die. The clearance, *t* is to be determined during the process design phase. *R1*, *R2,* and *t* are therefore independent optimization variables whereas *L1* and *Dw* are dependent variables.

In practice, almost all structural optimization problems involve constraints on optimization variables. Constraints define a feasible domain for variables. Selection of the constraint limits is usually based on the product requirements, the limitations on the process. If the feasible domain is arbitrarily restricted, better solutions are missed. Since there may not be a feasible geometry corresponding to an arbitrary set of values for the optimization variables, they are not free variables. For this reason, in this study, constraints are imposed on optimization variables based on the design and process requirements and possible instability sources in FE analysis. For fillet radius *R1*, the minimum allowable

value is 7.75 mm. which is equal to the radius of the punch. If both *R1* and *R2* are chosen to be 7.75 mm, the shape of the punch tip becomes spherical and smaller radii of curvatures may not be defined. On the other hand, there is no upper limit set for *R1*. If it tends to go to infinity, the tip becomes flat.

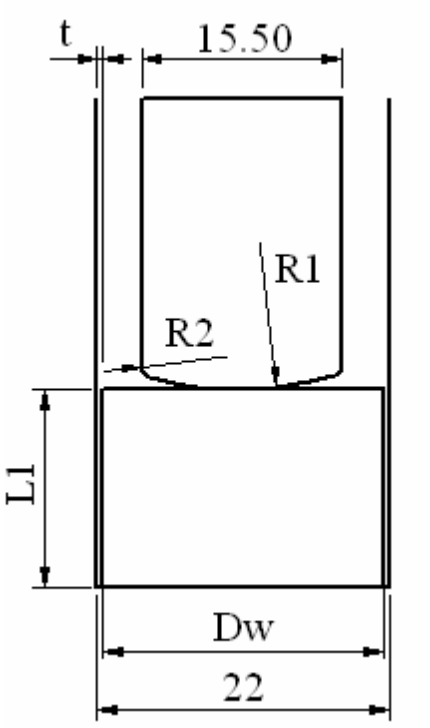

Figure 2.1. Die and workpiece geometries (dimensions are in mm)

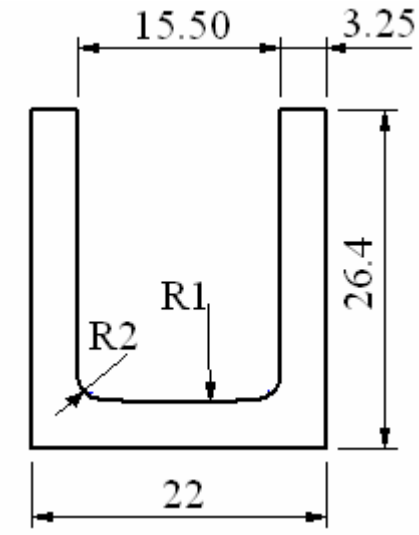

Figure 2.2. Geometry of the finished product (dimensions are in mm)

The upper limit for *R2* is 7.75 mm, which is the half of the punch radius. Beyond this upper limit, the curve defined by *R2* eliminates *R1*, and the punch tip becomes spherical. The lower bound of *R2* is 3 mm. A lower value may lead to difficulties in FE analysis. This limit is set due to a number of failed FE analyses below this value

In order to place the workpiece inside the die walls, the workpiece diameter should be smaller compared to that of the die walls. Because of this, a clearance 0.1 mm is taken as the lower limit of *t*. That means the workpiece should be machined to a diameter being at least 0.2 mm smaller than the diameter of the die walls. This constraint is an achievable value by means of manufacturing especially if CNC lathes are used. The upper limit of *t* is 0.5 mm. In practice, this limit is too large, since it may cause difficulties in workpiece positioning and uncertainties in deformation behavior. On the other hand, the feasible domain should be chosen as wide as possible, and should not be restricted based on the common practice. Otherwise, one may exclude the global minimum point from the feasible domain. As will be mentioned in Section 5, the upper limit of 0.5 mm is not active since results converge to the lower bound for the die gap *t*.

In order to minimize the variation in Vickers hardness using an optimization, an approach closer to that of Zhao and Wang [3] is used except that weighting factors are not utilized. Basically, the objective function is expressed as the sum of variations from an average Vickers hardness value. The theory of predicting the Vickers hardness value based on principal plastic strains is explained in the Section 3. Since plastic strains induced in a backward extrusion process are not analytically obtainable, thus FE analysis is utilized. Further details of obtaining principal strains and calculation method of the objective function are given in the Section 4.

3. THEORY OF HARDNESS AND STRAIN RELATIONS

A number of researchers [2, 8] have developed mathematical models to predict the hardness of cold formed products. These models are based on the relation between the hardness, properties of the raw material and the plastic strain induced during forming process. With the help of these models the resulting hardness characteristics of a cold formed product can be successfully predicted using the strain state determined through a finite element analysis.

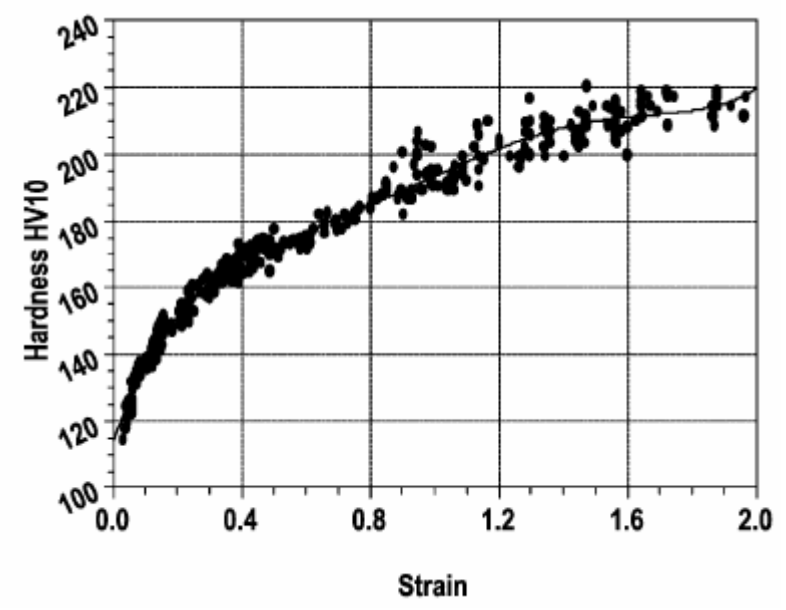

Figure 3.1. Local strain hardness curve for steel TRISTAL at 23 C [11]

The hardness, and thus the strength of a cold forged material increase with increased amount of permanent deformation. Figure 3.1 shows the relationship between the deformation and hardness of a steel specimen.

The increase in strength during the cold forging process is called strain hardening or work hardening. This phenomenon is explained by some micro-mechanisms. We know that the motion of dislocations allows plastic deformation. As dislocations move, it becomes more likely for them to encounter and interact with other dislocations or crystalline defects. As a result, an increased resistance to further motion develops. Moreover, mechanisms exist that markedly increase the number of dislocations in a metal during deformation, thereby enhancing the probability of interactions.

Since we define hardness as a measure of strength or resistance to plastic deformation, it can be stated that hardness also increases with increased amount of deformation [8]. Many studies were conducted in order to determine the correlation between deformation and hardness.

Kim *et al*. [10] stated that the hardness distribution in cold forged parts could be predicted if the hardness-effective strain relation of the material in use and the effective strain distribution of the finished part were known. In order to validate this assumption, they obtained hardness vs. effective strain curve for AISI 1010 steel by performing upsetting experiments, and they carried out FEM analyses to obtain effective strain. Then, they used these data to predict the hardness distribution in cold backward extruded cups.

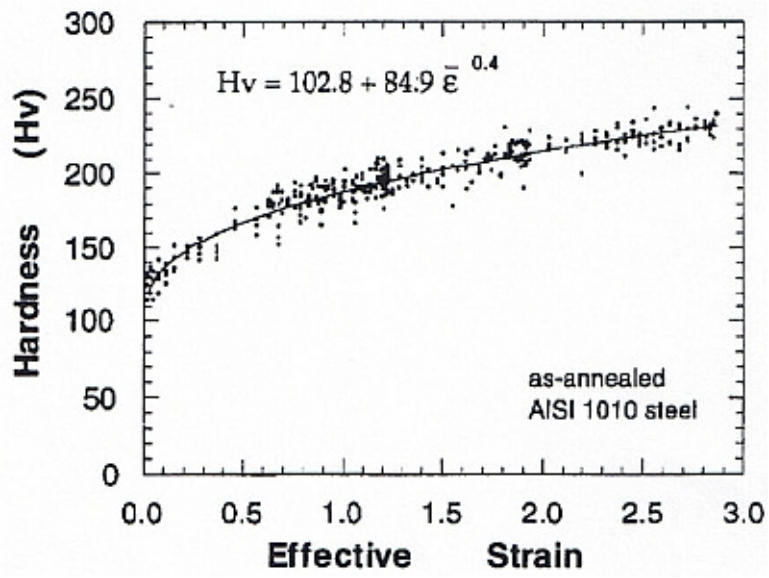

Figure 3.2. Hardness vs. Effective strain curve for AISI 1010 steel [10]

Kim *et al*. [10] performed upsetting analyses for grooved dies in order to create a wider effective strain distribution in the specimen compared to a non-grooved case. They assumed that the initial hardness distribution in the workpiece was homogeneous, the final hardness was a function of effective strain and not affected by the deformation history. They also assumed that the FEM analyses were reliable. After conducting upsetting experiments, they cut the specimens along their symmetry axis and measured hardness along the axial and radial lines of symmetry. Then, they simulated the upsetting experiments by FEM under the same conditions to obtain effective strains at the points, at

which hardness measurements were taken. They combined both results to obtain hardness and effective strain at several predetermined points in the specimens. Then, they plotted these predetermined points on hardness vs. effective strain chart (Figure 3.2). Lastly, they found a mathematical relation between the effective strain and Vickers hardness for AISI 1010 steel by curve fitting (Eq. 3.1).

$$HV = 102.8 + 84.9 \cdot \varepsilon^{-0.4} \tag{3.1}$$

At the second stage of the study by Kim *et al*. [10] they produced cold backward extruded cups made of AISI 1010 steel and conducted hardness measurements on the cups. Then they created a FE model of the process to obtain effective strain distribution of the specimens. Eq. 3.1 was used to calculate HV distribution from effective strain output of the FE analysis. Finally, the predicted and measured hardness values were compared and they were in good agreement.

At the second stage of the study by Kim *et al*. [10] they produced cold backward extruded cups made of AISI 1010 steel and conducted hardness measurements on the cups. Then they created a FE model of the process to obtain effective strain distribution of the specimens. Eq. 3.1 was used to calculate HV distribution from effective strain output of the FE analysis. Finally, the predicted and measured hardness values were compared and they were in good agreement.

Sönmez and Demir [8] proposed an analytical relation between the effective strain induced in a cold formed workpiece and the resulting Brinell or Vickers hardness. The significant point of this study is that the analytic relation between effective strain and hardness is constructed using flow curve constants, which are easily obtainable. In contrast, the model proposed by Kim *et al*. [10] (Eq. 3.1) uses constants specific for each material obtained through a series of time consuming experiments and numerical analyses.

Vickers hardness (*HV*) is defined as the load applied on a pyramidal indenter divided by the surface area of the permanent impression. Since the top angle of the pyramid is 136^{o}, and the pyramids base area is equal to 0.9272 times of its lateral area.

$$HV = 0.9272 \cdot Pm \tag{3.2}$$

where *Pm* is the mean pressure (the applied load *F*, over the projected area, *A*). The base area of the pyramidal impression *A*, is calculated by Eq. 3.3.

$$A = 2 \cdot s^2 \tag{3.3}$$

where *s* is the length of the base diagonal. *HV* is then given by

$$HV = 0.9272 \cdot \left(2 \cdot \frac{F}{s^2} \right) \tag{3.4}$$

Consequently, *HV* can be calculated if the diagonal of the indentation *s* is known.

Tabor [12] assumed that the stress developed at a certain point is representative of the whole deformation and it is linearly related to the average pressure.

$$Pm = \alpha \cdot \sigma_e \tag{3.5}$$

Here, α is a constant and σ_e is representative stress.

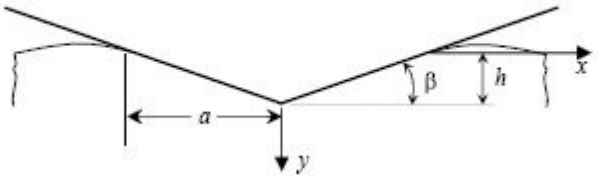

Figure 3.3. Geometry of a Vickers indentation [8]

Because a pyramidal indenter is used, if the magnitude of the acting force is increased, the depth of the impression changes whereas the impression shape remains unchanged. So the ratio h/a (the indentation depth/contact length) remains constant even if a deeper indentation occurs (See Figure 3.3). That makes $\varepsilon(x/a, y/a)$ independent of the indentation size. Representative yield strain (ε_e) corresponding to representative yield stress is independent of the load and hardness, and according to Tabor [12] it is equal to 0.08.

The true stress-true strain relation under uniaxial loading is described as

$$\sigma = K \cdot \varepsilon^n \tag{3.6}$$

where K and n are material constants.

The relation given by Eq. 3.6 is also valid for the representative stress and representative strain [8]. Thus, Eq. 3.6 becomes

$$\sigma_e = K \cdot \varepsilon_e^n \tag{3.7}$$

From Equations 3.2, 3.5 and 3.7

$$HV = c \cdot K \cdot \varepsilon_e^n \tag{3.8}$$

The constant c in Eq. 3.8, was obtained by Tabor [12] as 2.9. This equation is only valid for materials without any prior deformation. Since plastic strains are induced during a cold forging process, the effect of work hardening should be considered in the HV equation. Tabor found that the prior uniaxial plastic strain ε_o, could be added to ε_e. Eq. 3.8 then becomes

$$HV = c \cdot K \cdot (\varepsilon_o + \varepsilon_e)^n \tag{3.9}$$

Substituting the values of the constants, Eq. 3.9 may also be written as follows

$$HV = 2.9 \cdot K \cdot (\varepsilon_o + 0.08)^n \tag{3.10}$$

Sönmez and Demir [8] adapted this equation to 3D deformation problems, by substituting effective strain for ε_o in Eq. 3.10, which is given by

$$\varepsilon_o = \sqrt{\frac{2}{3} \cdot e_{ij} \cdot e_{ij}} \tag{3.11}$$

ε_{ij} is expressed as

$$\varepsilon_{ij} = e_{ij} = \begin{pmatrix} \frac{1}{3} \cdot (2\varepsilon_{11} - \varepsilon_{22} - \varepsilon_{33}) & \varepsilon_{12} & \varepsilon_{13} \\ \varepsilon_{21} & \frac{1}{3} \cdot (2\varepsilon_{22} - \varepsilon_{11} - \varepsilon_{33}) & \varepsilon_{23} \\ \varepsilon_{31} & \varepsilon_{32} & \frac{1}{3} \cdot (2\varepsilon_{33} - \varepsilon_{11} - \varepsilon_{22}) \end{pmatrix} \tag{3.12}$$

Substituting. 3.12 into Eq. 3.11 we obtain

$$\varepsilon_o = \sqrt{\frac{2}{3} \cdot (e_{11}^2 + e_{22}^2 + e_{33}^2 + 2 \cdot e_{11}^2 + 2 \cdot e_{13}^2 + 2 \cdot e_{23}^2)} \tag{3.13}$$

Effective strain as a function of principal strains, e_1, e_2 and e_3 is given by

$$\varepsilon_o = \sqrt{\frac{2}{3} \cdot \left(e_1^2 + e_2^2 + e_3^2\right)} \tag{3.14}$$

After having stated the analytical relation between the strain and Vickers hardness, Sönmez and Demir [8] performed upsetting experiments to find the flow curve constants for two different materials. Then, they conducted forward extrusion experiments and measured Vickers hardness at several points. They also simulated forward extrusion experiments using FE modeling to obtain effective strain distribution in the specimens, and then they calculated Vickers hardness using the analytical relation given by Eq. 3.9. At the end, comparison of experimental and predicted result showed a good agreement.

In this study, after determining the effective strain through FE analysis, Eq. 3.10 is used to calculate Vickers hardness.

4. METHODOLGY

The aim of this study is to develop a procedure to optimize the preform and die shapes to achieve desired hardness characteristics in a cold formed part. The procedure is applied to backward extrusion to obtain a uniform hardness distribution.

Firstly, the hardness distribution in the backward extruded part, which was described in the previous section, should be determined. As mentioned before, deformation (strain) induced in a cold forging processes increases the hardness of the workpiece. Fortunately, the effective strain and hardness can be related analytically as proposed by Sönmez and Demir [8]. This analytical expressed in Eq. 3.10 is employed in this study to determine the hardness distribution using numerically obtained effective strain distribution

In order to predict the change in hardness characteristics, the plastic strain distribution in the specimen induced by the backward extrusion process should be obtained. As a result of the complex and uneven deformation behavior of the workpiece, developed strains can not be found analytically. For this reason, a FE analysis is carried out to obtain the strain distribution. For this purpose, a commercial FEA software, ANSYS, is utilized. The reasons of this choice are the familiarity of the researcher with ANSYS, the well known reliability of the software, the applicability of optimization procedure using built-in programming language, and the flexibility in the presentation of outputs.

In the process optimization procedure, first of all, the objective function is analytically expressed. Then, the optimization variables and constrains are defined. The next step is to choose a proper search algorithm. In this study, Nelder-Mead algorithm was selected because it is a robust zero order search algorithm not requiring numerical derivatives of the objective function. To integrate the finite element model and the optimization algorithm, a built-in ANSYS code was developed. This program carries out FE analyses, writes the results into output files, and also evaluates the results to modify variables according to the decision criteria of the Nelder-Mead algorithm.

Figure 4.2 describes the methodology followed in this study. The details of finite element analyses and optimization are described in the following sections.

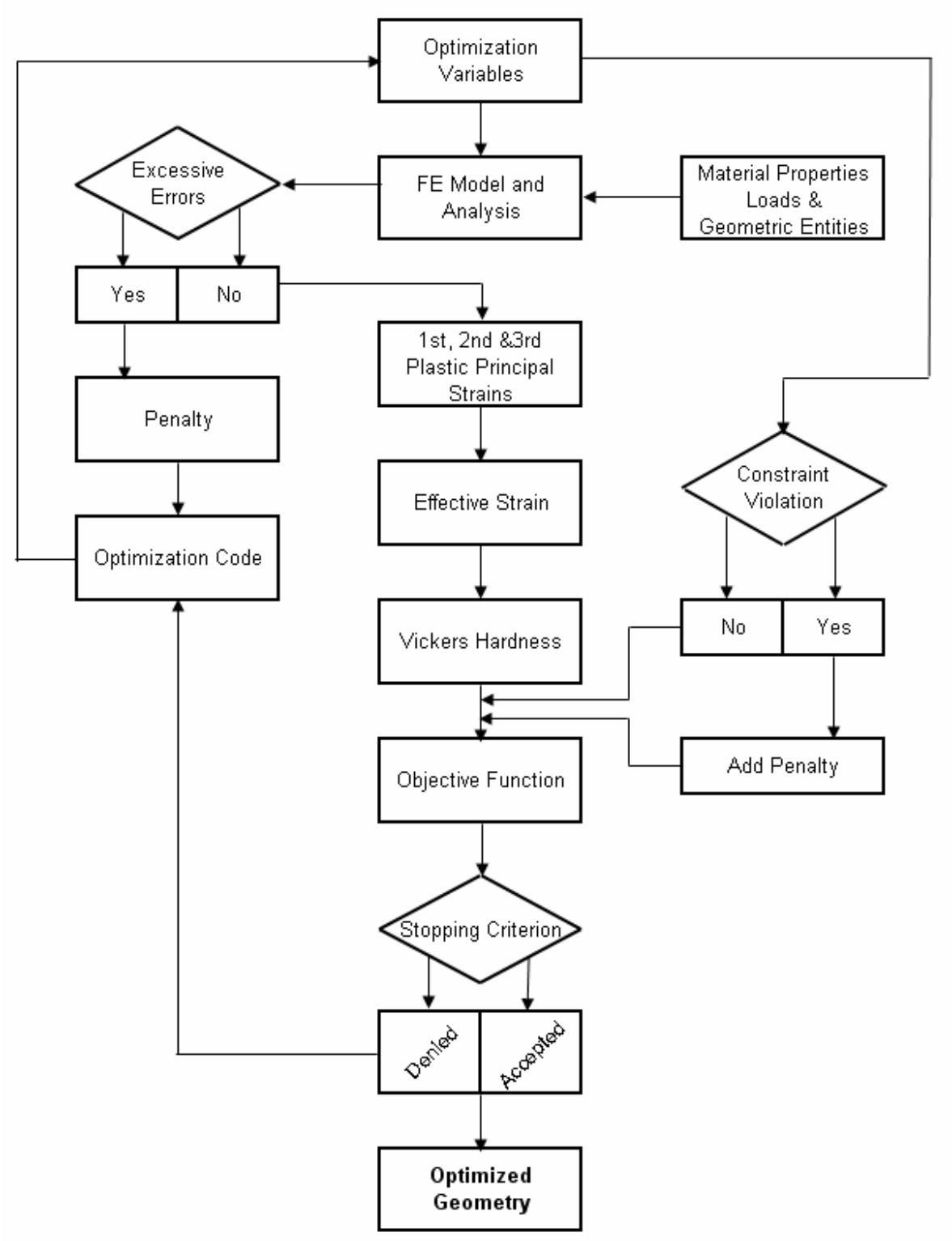

Figure 4.1. The optimization procedure

Initially, the optimization code selects random values for the optimization variables within the feasible domain and creates an initial geometry according to these selected values. Then, predefined loads, boundary conditions, material properties are defined in the finite element model. Following that, a finite element analysis is conducted, and first, second and third principal plastic strains are obtained. Using the plastic strain data, the code calculates the resulting effective strain by Eq. 3.14. To obtain Vickers hardness, Eq 3.10 and the calculated effective strain data are used. As mentioned before, the objective function is defined as the sum variation form the average Vickers hardness value. The details of the calculation method for the objective function are given in the following sections. Because, there are constraints on the optimization variables, this is a constrained optimization problem. In cases of constraint violations, a penalty is calculated and added to the value of the objective function. In this way, the problem is transformed to an unconstrained optimization problem. Penalties are activated under two conditions: firstly, if an optimization variable takes a value outside of its feasible range, and secondly, if the FE analysis fails. Further details of the penalty method are given in the section 4. Because the Nelder-Mead Algorithm requires k+1 configurations, k being the number of design variables, this procedure is repeated for four randomly created initial configurations. Having completed four FE analyses and obtained objective function values, the program compares these values according to the decision criteria of the Nelder-Mead Algorithm. This comparison leads to calculation of new values for the optimization variables and creation of a new geometry to be analyzed. In the Appendix D, the Nelder-Mead algorithm is explained in to its details. This procedure is repeated until the stopping criterion is satisfied, which requires the difference between the objective function values of the best and worst configurations to be small.

4.1. Optimization Procedure

Traditionally, manufacturing parameters are determined based on engineer's experience. In most cases, experience based selected parameters do not give satisfactory results. Thus, manufacturing parameters are modified according to outputs of a trial-error-correction phase. For manufacturing processes requiring high tooling costs, these trial and error efforts drastically decrease the efficiency of the process. The developments in the computer technology have started to change this traditional approach. Especially, FE

analysis allowed prediction of the effects of process parameters on the end product without actually producing it, which reduced trial and error efforts dramatically. On the other hand, FE analysis only provides outputs for a predetermined configuration and is not able to evaluate these outputs. Because of this, engineer is still responsible for finding a better configuration. In most applications, process' success depends on various parameters. Since FE analysis requires high computational costs, engineer does not have a chance to conduct a FE analysis to see effects of changes in each parameter. Thus a methodology is required to make feasible decisions. Today, a variety of optimization techniques to be combined with FE analysis are available in the literature. In short, the integration of optimization techniques with finite element analysis has pronounced effects on the product and process design. This integration allows reducing the design costs by shifting the burden from engineer to the computer. [13]

Definition of an optimization problem requires

- Determination of the objective function to be minimized
- Selection of design variables affecting the value of the objective function
- Setting the constraints
- Applying penalties, weighting constants
- Selection of optimization method.

After having selected the proper optimization algorithm, it is incorporated to an ANSYS command file. This command file automatically generates new configurations according to the algorithm and carries out the finite element analysis through the iterations and writes the results into an output file. After each iteration, the objective function is calculated unless the configuration yields no solution. Having calculated resulting value of the objective function, it is compared to the previous one. If the predetermined convergence criterion is satisfied, the algorithm is terminated and optimum values are obtained.

4.2. Objective Function

The optimization procedure requires an objective function to be minimized which is expressed in terms of the optimization variables. In this thesis, the objective is to obtain

optimum geometric parameters for the die and preform to minimize Vickers Hardness variation induced during the backward extrusion process. Thus, the degree of inhomogeneity should be defined analytically. Using variations of *n* number of elements from an average value is a frequently used method in the literature to evaluate variation of a physical entity.

The Vickers hardness is related to the effective strain as expressed in Eq. 3.10. Since FE results are obtained at the nodes, Eq. 3.10 is reformulated and given by

$$HV_i = 2.9 \cdot K \cdot \left(0.08 + \varepsilon_{oi}\right)^n \tag{4.1}$$

Here, HV_i is the Vickers hardness and ε_{oi} is the effective strain of the i^{th} node.

The average Vickers hardness within the extruded part, HV_{avg}, is given by

$$HV_{avg} = \frac{\sum_{i=1}^{n} HV_i}{n} \tag{4.2}$$

and *n* is the total number of nodes. One may define the deviation of the hardness at node *i* from HV_{avg} as

$$HVE_i = HV_{avg} - HV_i \tag{4.3}$$

The degree of inhomogeneity of hardness within the whole part is formulated as

$$HVE_T = \frac{\sum_{j=1}^{n} HVE_i^2}{HV_{avg}^2} \tag{4.4}$$

Note that HVE_T is defined as a power function to intensify the effect of deviation in hardness, and it is divided by HV_{avg}^2 for normalization.

The objective function is defined as

$$f(R1,R2,t) = w_1 \cdot HVE_T + w_2 \cdot \sum_{k=1}^{l} P_k + \eta \cdot P_a \tag{4.5}$$

Here, l is the number of applied constraint penalty functions.

During the optimization process, the value of the objective function is recalculated whenever optimization variables are changed by the search algorithm. For this purpose, non-linear FE analyses involving large deformation are performed. The search algorithm may generate a set of variables such that for some reason FE analysis fails, e.g. the geometry may not be constructed due to a negative value for radius of curvature. In that case, effective strain at node i (ε_{oi}) can not be calculated. ANSYS automatically assigns zero value for these parameters. According to Eq. 4.1 and Eq. 4.2, HV_{avg} and HV_i become equal to the hardness of the starting material. Consequently, the algorithm obtains zero variation in Vickers hardness and it sticks into this fake minimum point. In order to prevent this, an analysis error term, P_a, is defined. This error term should have a large value compared to other terms in the objective function so that it prevents converging into a fake minimum point. The analysis error term P_a becomes active, if FE analysis fails. P_a is used with a control coefficient η. In such a case, η is equal to 1.0 and the third term becomes nonzero. Otherwise, η is equal to zero.

In Eq. 4.5, w_1 is the weighting constant for HVE_T and it is equal to 1000, w_2 is the weighting coefficient for the penalties of constraint violations and it is equal to 10. For all penalty functions the same weighting constant is used since all optimization variables have about the same degree of importance in the objective function

Suppose that for the selected optimization variable, x, there exist a lower and upper bound denoted by x_l and x_u respectively. The inequality constraint is expressed as

$$x_l < x < x_u$$

This relation requires that two penalty functions be defined. For the lower bound, the penalty function is defined as

$$P_k = \left\langle \frac{-x + x_l}{x_l} \right\rangle \tag{4.6}$$

and the penalty function for the upper bound is

$$P_{k+1} = \left\langle \frac{x - x_u}{x_u} \right\rangle \tag{4.7}$$

Because the type of the penalty functions is external, they become active if their related constraint is violated. Otherwise, they are equal to zero. This activity is controlled by the operator "< >". If the value of the term inside this operator is positive, it yields the same value, otherwise it yields zero. Note that all penalty function are defined in a manner such that, they become less than zero, if their related variable takes a value from its feasible range.

For *R*1, there exists only one penalty function since it is constrained in one direction only whereas two penalty functions are required for both *R*2 and *t*, which are constrained in two directions. Consequently, five penalty functions are employed in the objective function.

4.3. Finite Element Modeling

Figure 4.3 shows a geometric representation of the punch, workpiece and dies in ANSYS. Note that an axisymmetric model is used instead of creating a 3D model, since use of an axisymmetric model greatly reduces the modeling and analysis time compared to that of an equivalent 3-D model for axisymmetric structures.

During the study, the FE model was created using batch files rather than graphical user interface, since this FE model was integrated in the optimization code. In this way, the FE analysis carried out and current optimization values are selected according to the search algorithm in each iteration through a single program without user intervention.

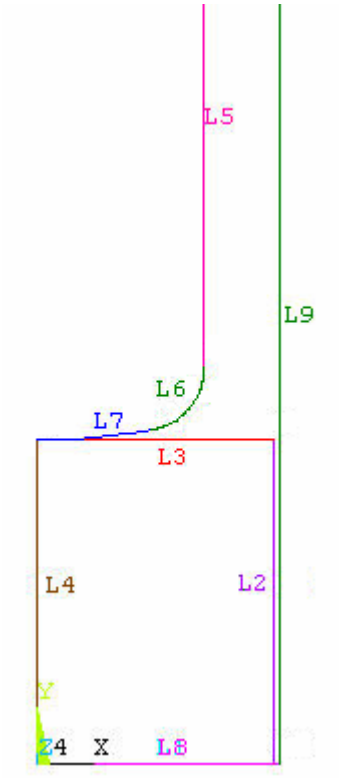

Figure 4.2. Workpiece, punch and die in ANSYS

4.3.1. Meshing

Selection of an appropriate finite element type is essential for obtaining reliable analysis results. Selected element should satisfy a set of requirements: Firstly, since axisymmetric approach is adopted in this study, the element type has to be compatible with axisymmetric modeling. Secondly, the element should have large deflection, large strain capabilities. Lastly, a high order element is more suitable for highly nonlinear deformation. Accordingly, the element type selected in this study is Plane183 being a high order, 8 node 2D rectangular element. ANSYS stores output data for corner nodes. Because of this, hardness value is only calculated at these four corner nodes (Nodes with labels *L, I, J* and *K* in Figure 4. 3).

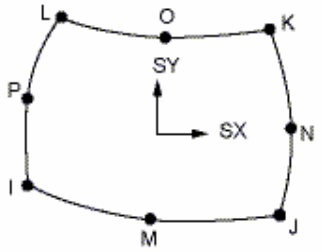

Figure 4.3. PLANE183 with its 8 nodes [14]

Assuming that the die and the punch do not undergo plastic deformation and their elastic deformations have a negligible effect on the deformation of the workpiece, their surfaces were defined as nondeformable by using rigid lines surrounding their representative areas, and thus they were not meshed. Only the workpiece was meshed. Consequently, the amount of mesh elements to be evaluated during the analysis was reduced, and the required solution time was decreased.

4.3.2. Creation of Contact Elements

The next step in the FE analysis was the creation of contact elements for the die-workpiece and punch-workpiece interfaces. The contact type used in this study was rigid-to-flexible and surface-to-surface contact. The dies and punch were defined as rigid target bodies whereas the workpiece was a deformable contact body. In order to establish contact pairs, the boundary lines of the bodies had to be meshed.

Table 4.1. Line numbers identifying contact pairs

Contacts		**Workpiece**				**Punch**			**Die**	
		L1	L2	L3	L4	L5	L6	L7	L8	L9
Workpiece	L1								X	
	L2									X
	L3					X	X	X		
	L4									
Punch	L5			X						
	L6			X						
	L7			X						
Die	L8	X								
	L9		X							

In our case, we had an axisymmetric 2D model with rigid-to-flexible, surface-to-surface contact. Under these conditions, CONTA172 was selected for deformable lines, and TARGE169 was selected for non-deformable lines. In order to create a contact, the groups of nodes which probably would come in contact with another one should be determined. Table.4.2 shows the line pairs between which contacts were defined. Line numbers are shown in Figure 4.2.

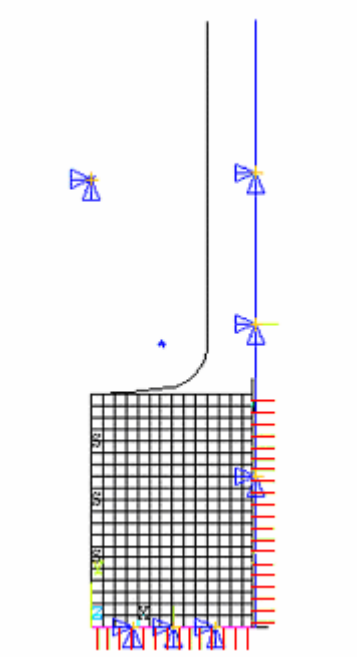

Figure 4.4. The FE model with its mesh, contact pairs and boundary conditions

4.3.3. Boundary Conditions

In the FE model, there are only displacement and axisymmetry boundary conditions applied on lines and nodes. The axisymmetry axis coincides with the line 4. The lines representing die walls are fixed in all degree of freedom (DOF). The punch lines are restrained from moving along the *x*-axis and rotation. They are only allowed to move through the prescribed vertical displacement. The punch movement along the *y*-axis is controlled with a pilot node. In Figure 4.4, the model with the applied boundary conditions is shown. Between the contacting surfaces, friction forces exist.

4.3.4. Friction Factor

In the literature, one of the proposed methods to determine the friction constant for die-workpiece interface to be used in modeling of backward and forward extrusion processes was to conduct ring compression tests. Gouveia *et al*. [15] conducted FE simulations of forward extrusion process. They utilized Coulomb friction model with a constant friction factor of 0.18 which was obtained by ring upsetting experiments. Having conducted finite element analysis of the process, they carried extrusion experiments to validate their model. Experimental measurements showed that the friction factor was not in agreement with the expectations from the ring compression test. Consequently, they stated that this disagreement might be caused by differences in the deformation behavior and the pressure, and they also stated that applying a lower friction factor would give theoretical results closer to that of experiments.

Hur *et al*. [9] simulated backward extrusion process. The friction coefficient m was assumed to be constant and equal to 0.1. Petruska and Janicek [11] studied strain inhomogeneity through hardness measurements on cold formed products. The type of the forming process they considered was forward extrusion. They simulated friction by Coulomb's model, and the friction factor was equal to 0.15. Roy *et al*. [7] simulated extrusion process of automotive outer race preforms. They applied a constant friction factor of 0.1 in their FE model.

In this study, Coulomb's model was assumed to correctly reflect the friction at the die-workpiece and punch-workpiece interfaces as in the previous studies. However, there is no clear agreement on the value of the friction factor m. In practice, friction factor may depend on the type of the materials in contact, but it may also vary due to varying lubrication and surface conditions even if the same types of die and workpiece materials are used. In this study, the friction constant was assumed to be 0.1, which was within the range of values adopted in the previous studies.

In order to observe the effects of variations in the friction factor, a number of FE simulations were conducted. The results are given in Table 4.1. The change in the friction coefficient from 0.1 to 0.08 resulted in a reduction of 8.9 per cent in the objective function

value. On the other hand, if it was changed to 1.2, a 8.6 per cent increase was observed. The difference between the objective function values of the cases with friction factors 0.06 and 0.12 was about 27.5 per cent. Consequently, it can be stated that the friction factor *m* should be minimized to obtain a more uniform hardness distribution, which indicates the importance of lubrication in cold forging processes.

Table 4.2. Effect of friction on the objective function

Nr	Friction Factor *m*	*f*
1	0.06	10.107
2	0.08	10.726
3	0.1	11.776
4	0.12	12.885

4.3.5. Material Model

In ANSYS, there are several alternatives to model the material properties. In this study, the selected material model is multi-linear isotropic hardening (MISO) model. MISO is a rate independent model suitable for large strain applications.

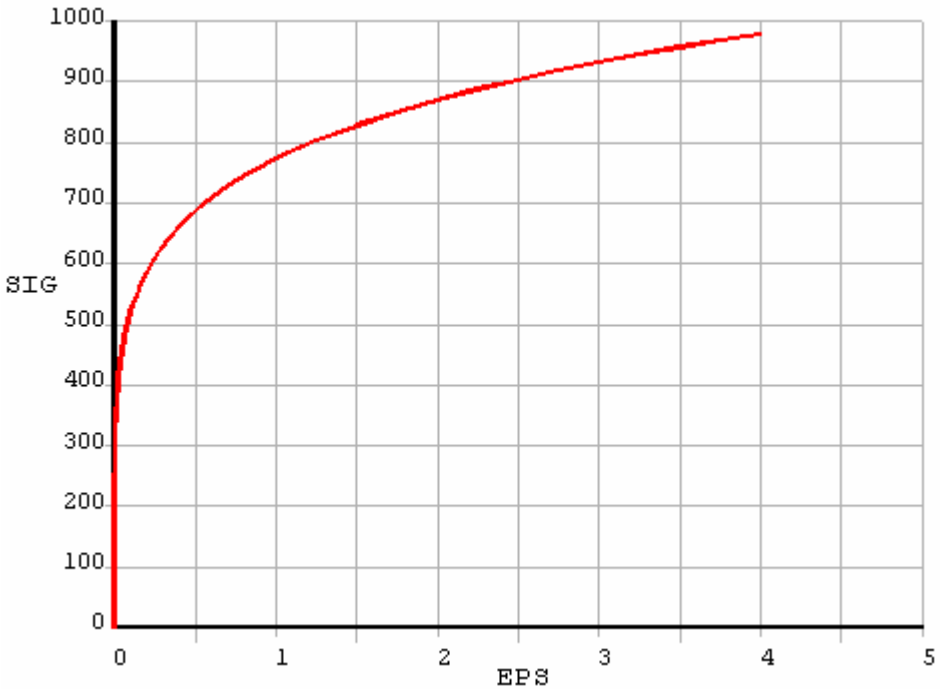

Figure 4.5. MISO flow curve of St37 generated in ANSYS

In MISO, the stress-strain curve is described by a set of linear sub-elements, instead of a power equation. To define the strain-stress curve to be used in the nonlinear analysis, datum points from the stress-strain curve are required. The more points are entered, the better the non-linear behavior is approached. The MISO flow curve of ST37 created by ANSYS using the given points is shown in Figure 4.5. This curve is defined by 38 datum points from the materials flow curve. These points are given in Appendix C.

4.3.6. Convergence Analysis of the FE Model

The solution settings such as the total number of iterations or the number of load steps affect the results dramatically. In most cases, ANSYS warning massages generated by ANSYS guide to find the proper solution settings. For plastic deformation analysis, improper settings may cause excessive deformations in mesh elements, FE formulation errors or convergence failures. After a trail and error phase, the proper settings were obtained. Not only solution settings, but also mesh element size are important for the reliability of the FE analysis. In order to check the reliability of the backward extrusion model, a convergence analysis was conducted. Under the conditions described above (geometry, boundary conditions, etc.) the analysis was repeated for mesh sizes from 1 to 0.1. The convergence analysis was reapplied for applied displacements of 4.0, 6.0 and 8.0 mm. Corresponding results are given in Tables 4.3, 4.4 and 4.5. Note that the convergence of the FE results was checked based on the maximum values of the selected output type.

Note that the maximum Vickers hardness variation for 4, 6, and 8 mm displacements (with corresponding to 0.266, 0.4, 0.533 displacement/workpiece length ratio) are 0.93, 0.98, and 3.49 per cent respectively. The convergence analysis results show that the increase in the HV variation is caused by the increased amount of strain. On the other hand, for mesh sizes below 0.4, the maximum variation is reduced to 1.29 per cent. In Vickers hardness scale, this error is negligible. Tables 4.3, 4.4 and 4.5 prove the convergence of the analyses results.

Table 4.3. Convergence analysis results for 4 mm applied displacement

Esize	Max HV	Diff	%Diff
1	Failed	Failed	Failed
0.8	205.481	-	-
0.7	205.602	0.121	0.059
0.6	207.508	1.906	0.927
0.5	207.762	0.254	0.122
0.4	209.227	1.466	0.705
0.3	209.824	0.597	0.285
0.2	210.942	1.118	0.533
0.1	211.052	0.11	0.052

Table 4.4. Convergence analysis results for 6 mm applied displacement

Esize	Max HV	Diff	%Diff
1	230.341	-	-
0.8	232.530	2.189	0.95
0.7	234.128	1.599	0.688
0.6	236.010	1.882	0.804
0.5	235.546	0.464	-0.197
0.4	237.858	2.312	0.982
0.3	239.162	1.304	0.548
0.2	241.513	2.350	0.983
0.1	243.060	1.547	0.226

Table 4.5. Convergence analysis results for 8 applied mm displacement

Esize	Max HV	Diff	%Diff
1	247.400	-	-
0.8	250.588	3.188	1.29
0.7	259.340	8.752	3.49
0.6	253.486	-5.855	-2.26
0.5	253.274	-0.212	-0.08
0.4	254.651	1.377	0.54
0.3	254.752	0.101	0.04
0.2	258.04	3.289	1.29
0.1	259.184	1.144	0.44

The backward extrusion process was simulated using the trial values of 30, 3, and 0.2 mm for *R1*, *R2*, and *t* respectively. Prior to the start of the optimization process, a FE analysis was conducted with the given initial configuration. Outputs of this analysis are given in Figures 4.6-13. Figure 4.6 shows the deformed mesh and undeformed workpiece

under edge. Note that mesh distortion is largest in the corner defined by *R2*. A closer view of this corner is shown in Figure 4.7. Figures 4.8, 4.9 and 4.10 display first, second and third principal strains develop in the workpiece. The effective strain distribution is given in Figure 4.11. Corresponding Vickers hardness distribution is shown in Figure 4.12. Finally, Figure 4.13 shows the hardness variance from the average Vickers hardness of the backward extruded part.

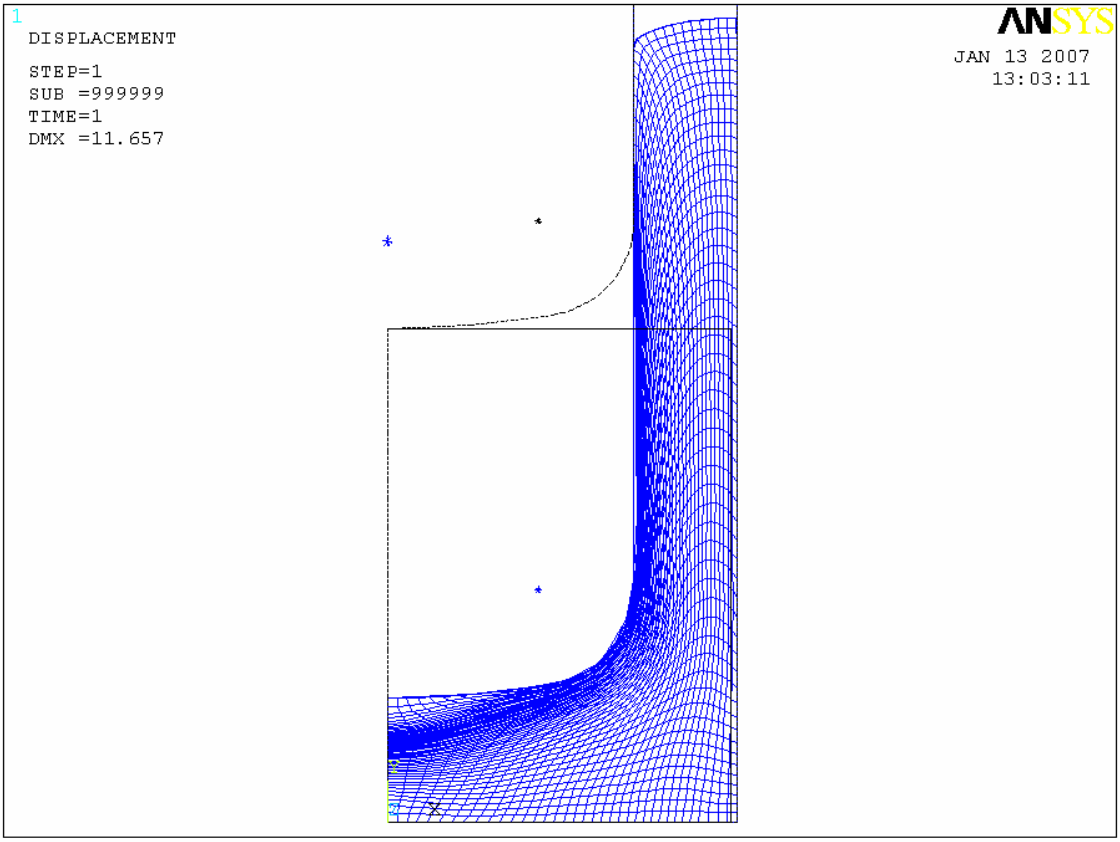

Figure 4.6. Deformed mesh

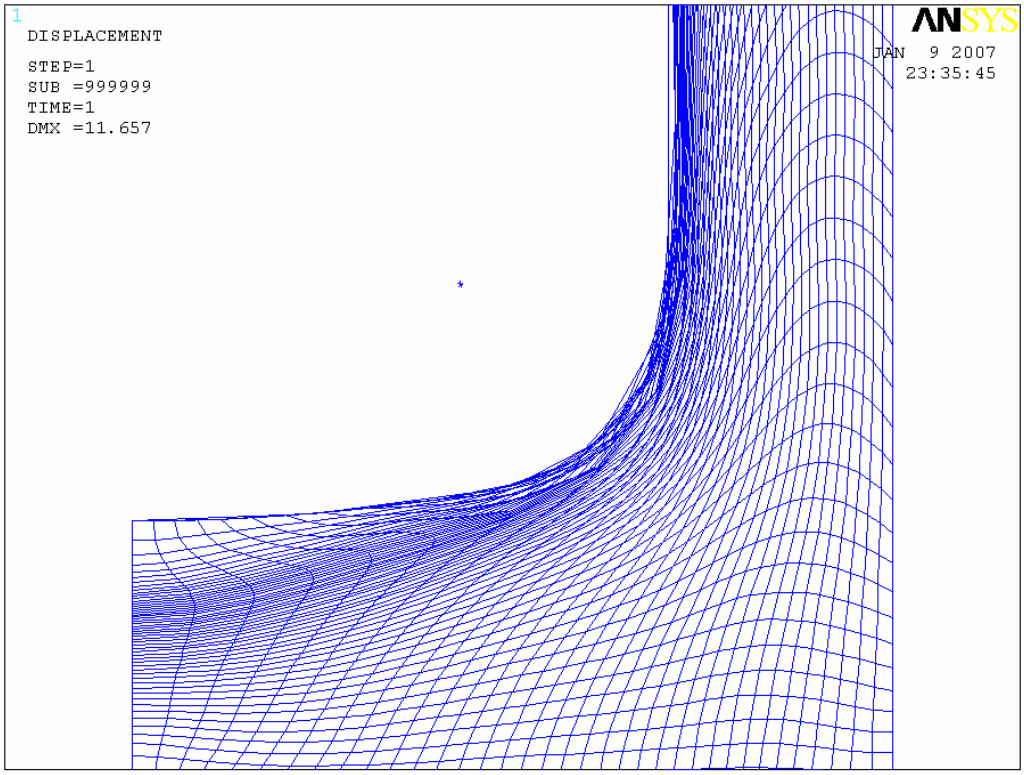

Figure 4.7. Deformed mesh in detail

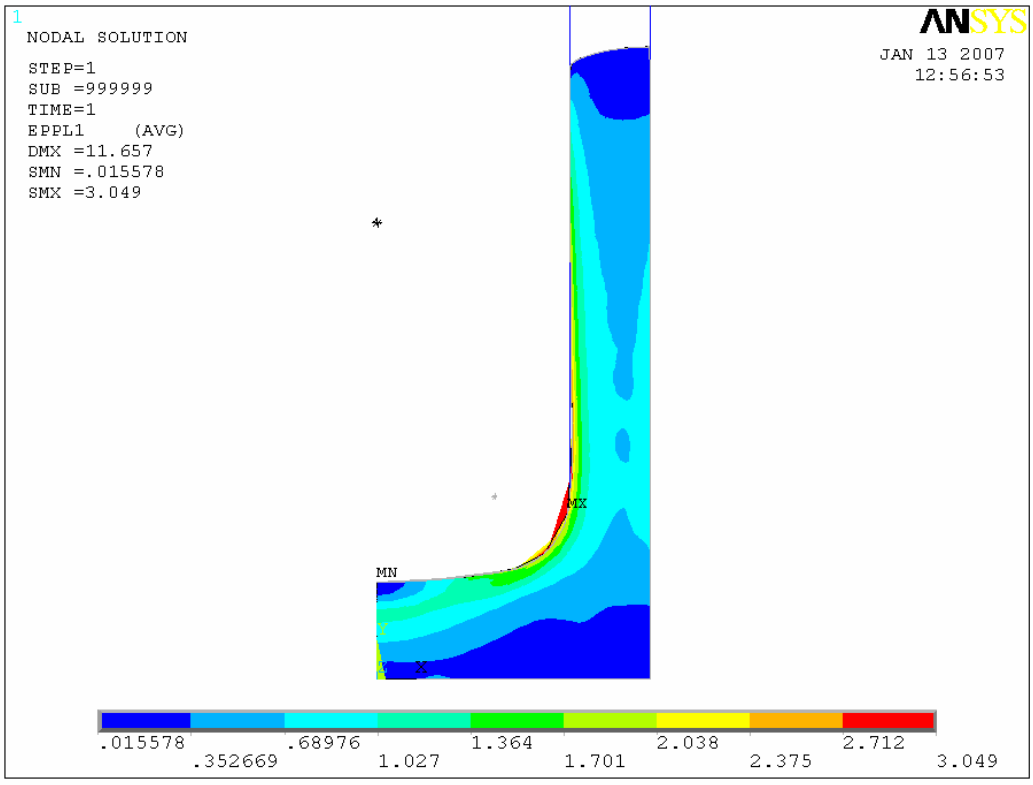

Figure 4.8. 1st principal plastic strain

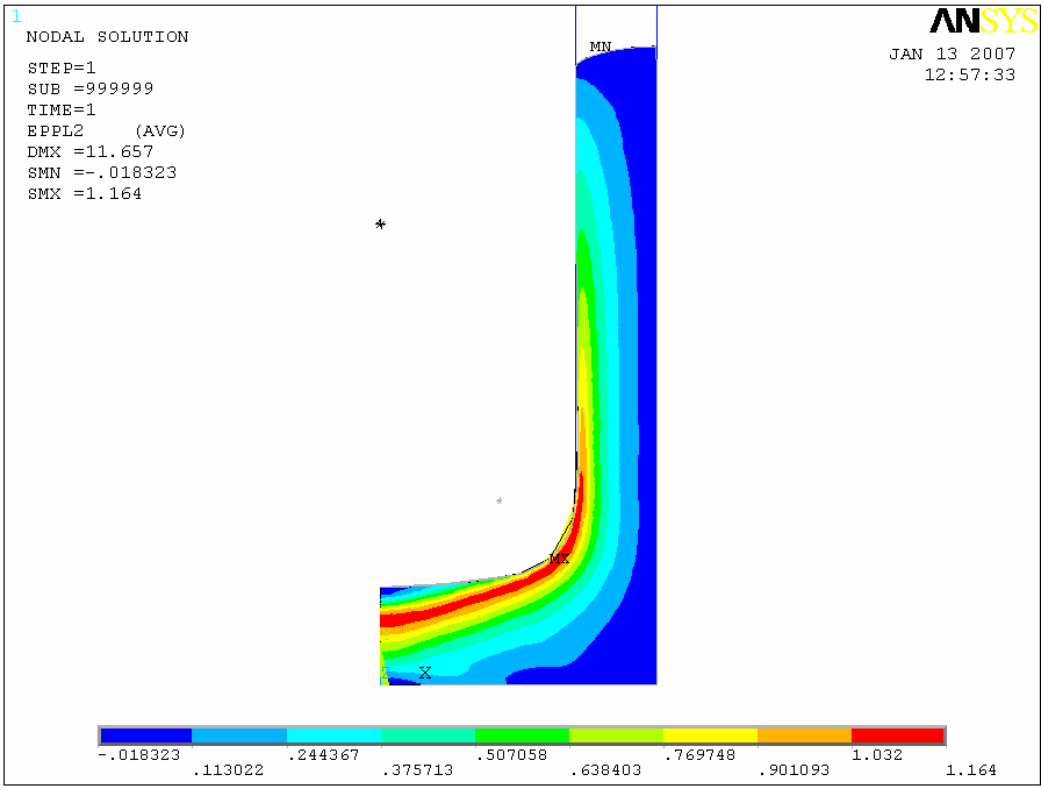

Figure 4.9. 2nd principal plastic strain

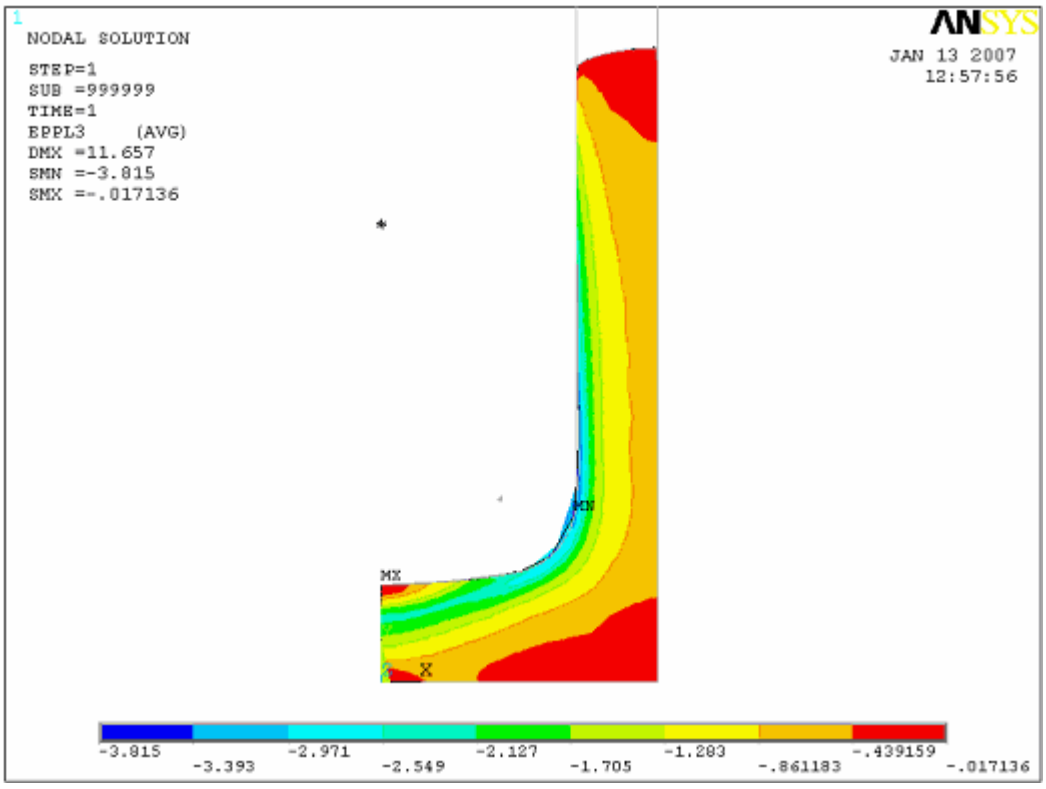

Figure 4.10. 3rd principal plastic strain

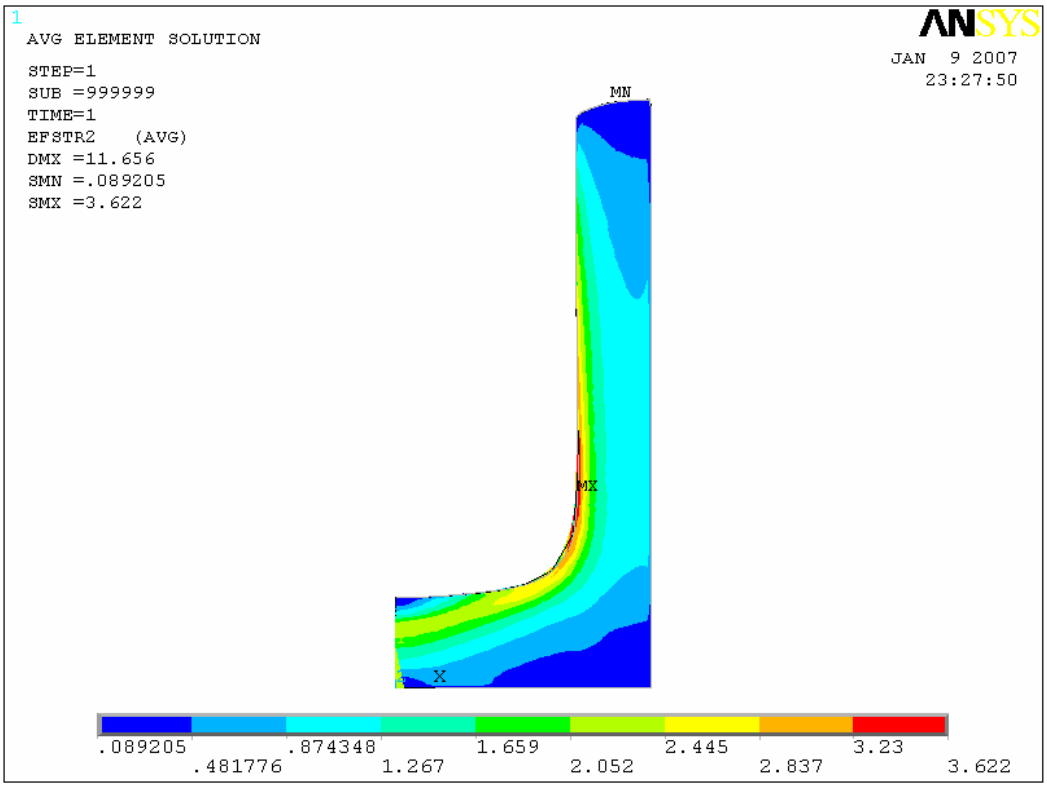

Figure 4.11. Effective strain distribution

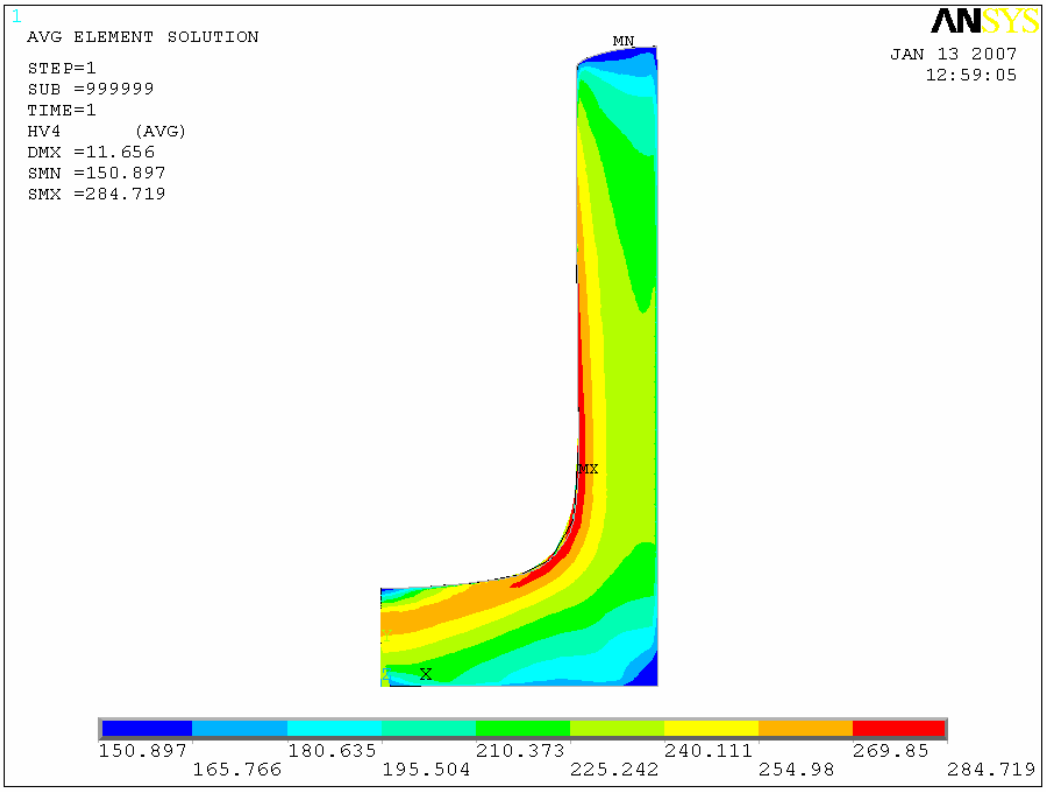

Figure 4.12. Hardness Distribution

5. RESULTS AND DISCUSSIONS

5.1. Evaluation of Constraints

Selection of optimization variables and determination of constraints are explained in the previous sections. After having developed the optimization code to be run in ANSYS environment, a group of optimization iterations were conducted. Optimization results showed that variables might tend to converge to their either upper or lower limits. In this case, initially chosen feasible domain may be extended to search for better configurations beyond these limits unless this violates design requirements, process restrictions and other criteria related to the computational difficulties etc. If a variable is monotonically increasing to its upper limit, or monotonically decreasing to its lower limit during the optimization process, one may assign this limit value to the parameter assuming that this is the optimum value for this parameter; it thus becomes a constant in the following optimization runs. In this way, the global minimum can be located more easily and computational cost can be decreased.

Table.5.1. gives the vertices of the initial simplex of the first run. All dimensions are given in mm. The final vertices obtained after optimization are given in Table 5.2. A second run is conducted under the same conditions with a different set of starting variable values. These values are presented in Table.5.3. Obtained result set of the second run is given in Table 5.4.

Table 5.1. Initial vertices of the 1st run

	R1	***R2***	***t***	***f***
1	30.891	5.585	0.291	15.599
2	57.974	4.140	0.174	13.136
3	15.874	5.059	0.495	15.558
4	53.388	4.302	0.386	14.171

Table 5.2. Final vertices of the 1st run

	R1	***R2***	***t***	***f***
1	77.919	3.004	0.111	11.437
2	78.000	2.996	0.109	11.429
3	78.273	3.005	0.105	11.435
4	77.465	2.993	0.109	11.438

Table 5.3. Initial vertices of the 2nd run

	R1	*R2*	*t*	*f*
1	85.468	5.075	0.309	14.874
2	102.921	4.007	0.235	13.320
3	43.702	5.585	0.291	15.583
4	85.780	4.140	0.174	13.156

Table 5.4. Final vertices of the 2nd run

	R1	*R2*	*t*	*f*
1	109.734	3.005	0.124	11.574
2	109.645	3.008	0.123	11.574
3	110.309	2.992	0.122	11.583
4	109.961	2.995	0.122	11.574

Remember that the constraints for $R1$, $R2$ and t are as given below.

$$7.75<R1$$

$$3<R2<7.75$$

$$0.1<t<0.5$$

Note that t and $R2$ converge to their lower boundary in the first and second runs (see Table 5.2 and Table 5.4). For this reason, the corresponding constraints and penalty functions are modified as will be discussed in the following section.

In contrast to $R2$ and t, $R1$ does not show a tendency to converge to its lower bound (remember that $R1$ has a lower bound only). Therefore, optimization is continued without any modification on the constraint and corresponding penalty function of $R1$.

5.2. Optimum Values of Design Variables

5.2.1. Die Gap *t*

A minimum value should be set for die gap t, because the workpiece diameter has to be smaller than the die cavity in order to be placed inside of it. Billets to be used as workpiece are available in standard sizes in the market. Thus, billets are generally machined by material removal processes to obtain workpieces with desired geometric

properties. At the initial phases of the optimization, the smallest allowable value of *t* was taken as 0.1 mm. Since *t* converged to its minimum limit, we tried to extend the feasible range to 0.05<t<0.5. However, in this case the preform should be machined to a higher degree of precision in order be able to force into the die without difficult, and this will increase the manufacturing cost. Using the new lower bound for *t*, the optimization process was repeated with the initial vertices given in Table.5.5. As shown in Table 5.6 *t* again converged to its minimum. Note that although *R*1 and R*2* converged to the same values (109 and 3 respectively) as shown in Tables 5.4 and 5.6, the optimum objective function value is smaller for the smaller lower limit. This shows that choosing a smaller clearance is conducive to more uniform hardness distribution.

Table 5.5. Initial vertices for the case 0.05<*t*<0.1

	R1	***R2***	***t***	***f***
1	111.163	5.075	0.309	14.872
2	136.835	4.007	0.235	13.341
3	56.514	5.585	0.291	15.574
4	113.586	4.140	0.174	13.171

Table 5.6. Final vertices for the case 0.05<*t*<0.5

	R1	***R2***	***t***	***f***
1	107.467	3.020	0.051	11.194
2	108.587	3.008	0.051	11.190
3	108.617	2.994	0.050	11.194
4	109.080	2.994	0.050	11.196

The lower constraint of *t* was further shifted to 0.01 mm. The same initial vertices were used as in the previous case. Only penalty functions were updated according to the new domain of *t*. The resulting vertices and corresponding objective function values are given in Table 5.7.

Table 5.7. Final vertices for the case 0.01<*t*<0.5

	R1	***R2***	***t***	***f***
1	82.392	3.008	0.011	10.868
2	82.467	3.001	0.010	10.865
3	82.246	3.017	0.010	10.886
4	82.934	3.001	0.010	10.867

For 0.01<*t*<0.5, *t* converged again to its lower bound, 0.01, as seen in Table 5.7. One may not choose a smaller clearance, because this requires too tight machining tolerances for billets, unless increased machining costs can be tolerated.

In order to validate the approach given above, another optimization run is conducted with initial vertices given in Table 5.8. Corresponding results are given in Table 5.9.

Table 5.8. Initial vertices for the case 0.01<*t*<0.1, second run

	R1	***R2***	***t***	***f***
1	136.835	4.007	0.235	13.341
2	56.514	5.585	0.291	15.574
3	113.586	4.140	0.174	13.171
4	24.870	5.059	0.495	15.419

Table 5.9. Final vertices for the case 0.01<*t*<0.5, second run

	R1	***R2***	***t***	***f***
1	210.174	3.002	0.012	11.008
2	211.558	3.006	0.011	11.006
3	210.015	3.000	0.011	11.001
4	208.545	3.002	0.010	11.000

One may conclude that, the theoretical optimum value of *t* is tending to approach zero. In practice, the optimum value of *t* is the tightest tolerance allowed by the manufacturing process used for preparing the workpiece. In this study, *t* is supposed to be 0.01 mm. From this point on, it becomes a constant, and it is not evaluated in further optimization runs. As a result, the optimization problem is simplified from 3D to 2D.

5.2.2. Corner Radius *R*2

Tables 5.2, 5.4, 5.6, 5.7 and 5.9 show that *R2* converges to 3.0, as *t* converges to its minimum allowed value. Because the value for the lower limit of R2 was chosen in order to avoid difficulties that sharp corners may cause in finite element calculations and also wearing away of the punch after repeated use, we may assume that there is a leeway to relax this constraint also. But first, a new optimization run, was conducted with the die gap *t* having fixed to 0.01 mm. Then, only two geometric variables remain with the starting values given in Table.5.10.

Table 5.10. Initial vertices for the case 3<*R2*<7.75

	R1	***R2***	***f***
1	66.822	5.385	13.820
2	89.593	5.235	13.587
3	136.835	4.007	12.141

The results of the completed run are given in Table.5.11. It is observed that *R2* converges to 3.0 as in the previous cases.

Table 5.11. Final vertices for the case 3<*R2*<7.75

	R1	***R2***	***f***
1	167.801	3.003	10.991
2	168.759	2.997	10.996
3	166.833	2.998	10.994

After having ensured that the optimum value for *R2* does not lie close to its maximum boundary, the upper limit was shifted to 5.0 mm whereas the new lower limit was chosen to be 2.0 mm. Another optimization run was conducted using these new limits with the initial vertices given in Table.5.12. Corresponding results are shown in Table.5.13.

Table 5.12. Initial vertices for the case 2<*R2*<5

	R1	***R2***	***f***
1	66.822	4.077	12.174
2	89.593	3.854	11.850
3	136.835	2.010	9.949

Table 5.13. Final vertices for the case 2<*R2*<5

	R1	***R2***	***f***
1	136.788	2.012	9.950
2	137.049	2.005	9.946
3	136.835	2.010	9.949

Results given in Table 5.13 show that *R2* again converges to its lower limit. Then, the limits of *R2* were revised as 1.5 and 4 mm, and the optimization process was repeated

Table 5.14. Initial vertices for the case 1.5<*R2*<4

	R1	***R2***	***f***
1	79.170	2.301	10.229
2	128.443	2.955	10.928
3	113.586	1.675	9.750

Table 5.15. Final vertices for the case 1.5<*R2*<4

	R1	***R2***	***f***
1	36.176	1.515	9.340
2	36.185	1.515	9.342
3	36.173	1.515	9.339

Table 5.11 shows that *R2* converges to 1.515 mm. This result implies that *R2* tends to converge to the minimum possible value allowed by its constraints. On the other hand, too small *R2* values may lead to stress concentration, shorter tool life and decreased reliability of FE results because of poor convergence. Accordingly, 2.0 mm is considered as a suitable value of *R2*.

In the following analysis, *R2* becomes a constant parameter instead of being an optimization variable. Consequently, the remaining optimization variable is *R1*. The optimization problem becomes a one dimensional problem, which decreases computational effort.

5.2.3. Bottom Radius *R*1

Optimum values of die gap *t* and punch corner radius *R2* were obtained in the previous runs. As mentioned above, optimum values of *t* and *R2* are 0.01 and 2.0 mm respectively. Having obtained the optimum values of *R2* and *t*, the remaining optimization variable is the punch bottom radius *R1*. Following runs were conducted to obtain the global optimum value of *R1*. Since the optimization problem was simplified as a result of decreased number of variables, required computational time was also decreased. That allows trying more initial sets of vertices which increases the possibility of obtaining the globally optimum configuration.

Table 5.16. Optimization results for *R1*

		Initial Simlex		Final Simlex	
Run Nr.	**Vertex Nr.**	***R1***	***f***	***R1***	***f***
1	**1**	113.163	9.868	83.701	9.805
	2	89.593	9.806	86.647	9.805
2	**1**	101.828	9.836	85.966	9.805
	2	136.835	9.899	86.513	9.804
3	**1**	8.257	17.549	31.525	9.573
	2	79.170	9.809	31.248	9.573
4	**1**	79.170	9.809	45.335	9.695
	2	56.514	9.795	45.324	9.695
5	**1**	8.000	18.007	31.438	9.573
	2	200.000	9.917	31.250	9.573

The results of the optimization runs that which were carried out to find the optimum value of *R1* are given in Table 5.16, which shows that the optimum value of *R1* is between 31.525 and 31.248. In this interval, the change in the objective function value is less than 0.001. Thus, the optimum value of *R1* may be assumed to be 31.5 mm.

Table 5.17. Optimization results for *R1*>100

Run Nr.	***R1***	***R2***	***t***	***f***
1	104.000	2.000	0.010	9.843
2	136.835	2.000	0.010	9.899
3	152.000	2.000	0.010	9.904
4	200.000	2.000	0.010	9.917

Values given in Table 5.17 were selected from the results of different runs, in which *R1* exceeded 100 to show that beyond 100 mm, the more *R1* is increased, the higher objective function results are obtained. In addition, for the values of *R1* higher than 200 mm, the curvature on the punch tip becomes nearly flat. Thus, a dramatic change in the objective function values is not expected beyond this limit. One should also note that the objective function is not very sensitive to changes in R2 when it is large. Thus, if the bottom should be almost flat as a design requirement, the increase in the objective function will not be large.

5.3. Evaluation of the Results

The optimum values of *R1*, *R2*, and *t* are found to be 31.5, 2 and 0.01 mm respectively. These values of the optimization variables result in an objective function value of 9.573. The worst four configurations and their resulting objective function values are given in Table 5.18. The worst one is 18.007. There is about 46.8 per cent reduction in the variation of the Vickers hardness distribution, which is a dramatic improvement between the worst and the best case.

In the best case, the highest and lowest Vickers hardness values are 284.73 and 148.75, whereas the extremum values in the worst case are 286.809 and 148.95. Because our objective is to reduce variation in hardness, not its maximum value, it can be stated that the applied procedure has a little effect with regard to decreasing the maximum hardness value or the difference between that of the highest and the lowest.

Table 5.18 The worst four configurations

Run Nr.	*R1*	*R2*	*t*	*f*
1	8.000	2.000	0.010	18.007
2	8.257	2.000	0.010	17.549
3	57.774	5.553	0.309	17.061
4	30.891	5.585	0.291	15.599

Note in Table 5.18 that the worst two objective function values were obtained using the optimum values of *R2* and *t* which shows the sensitivity of the objective function to *R1* near its lower bound. In contrast, this sensitivity to *R1* decreases when it takes a large value as indicated before. For instance, for two different values of *R1* (83.701 and 86.647 given in Table 5.12), the same objective function value is obtained (9.805), although there is a 3.5 per cent difference between them. On the other hand, a change in *R1* from 8 to 8.257 (3.2 per cent difference) resulted in an increase of 2.6 per cent in the objective function value.

Although the objective function is sensitive to *R1* near its minimum bound, the effects of *R2* and *t* can not be neglected. For the case that *R1* is equal to 30.891 mm, which is close to its optimum value, the corresponding function value is 15.599, which is the fourth worst result in the whole optimization procedure. This result was due to the values

of *R2* and *t* being far from their optimum value. Previously, it was mentioned that the weights of *R1*, *R2* and *t* were assumed to be same. The results show that this assumption is correct.

In Figure 5.1 and 5.3, Vickers hardness distribution plots are given for the best and worst geometries respectively. Figure 5.2 shows the variation of Vickers hardness from the average hardness value for the optimum geometry and Figure 5.4 shows that of the case causing the largest hardness variation.

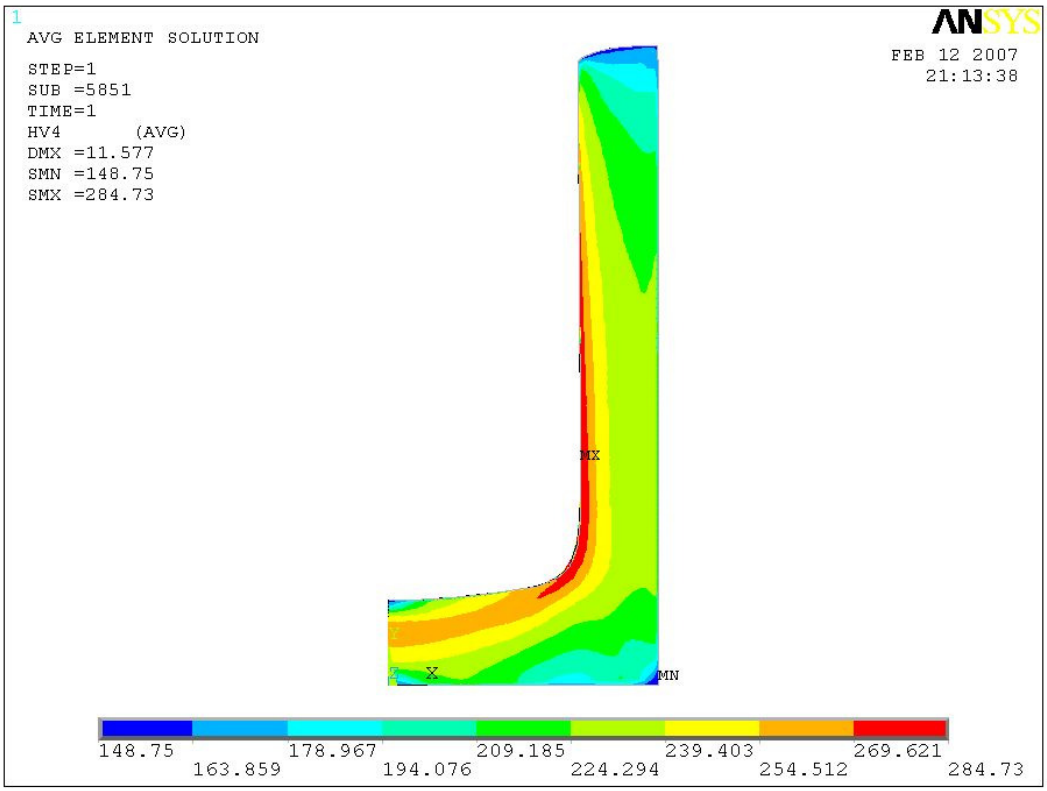

Figure 5.1. The optimum Vickers hardness distribution

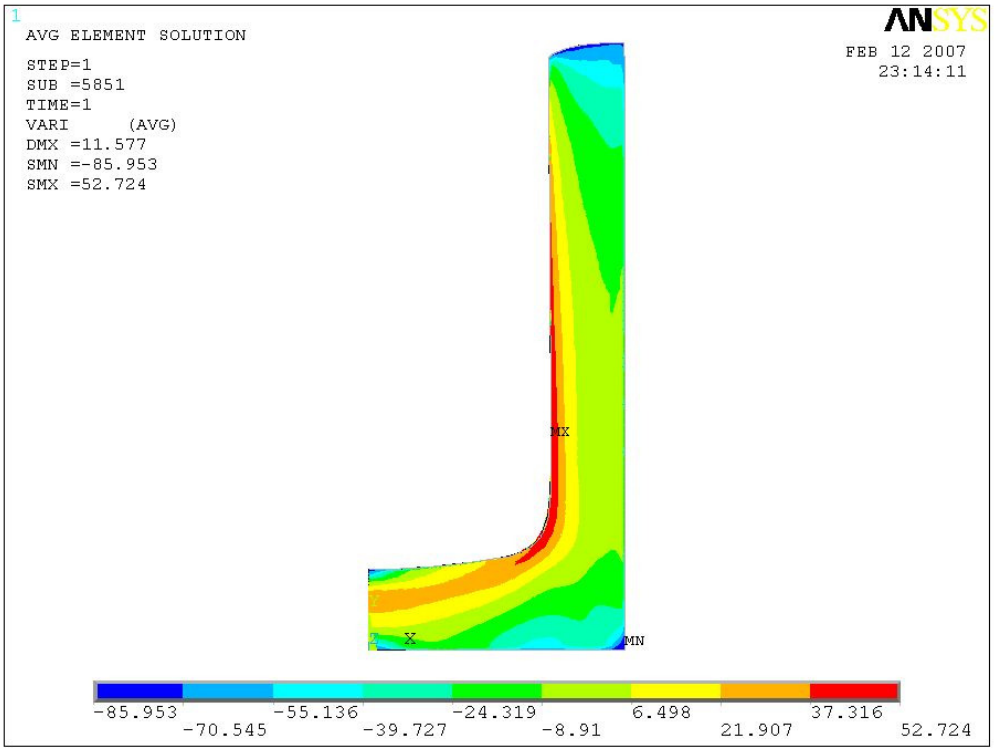

Figure 5.2. The variation in Vickers hardness for the optimum shape

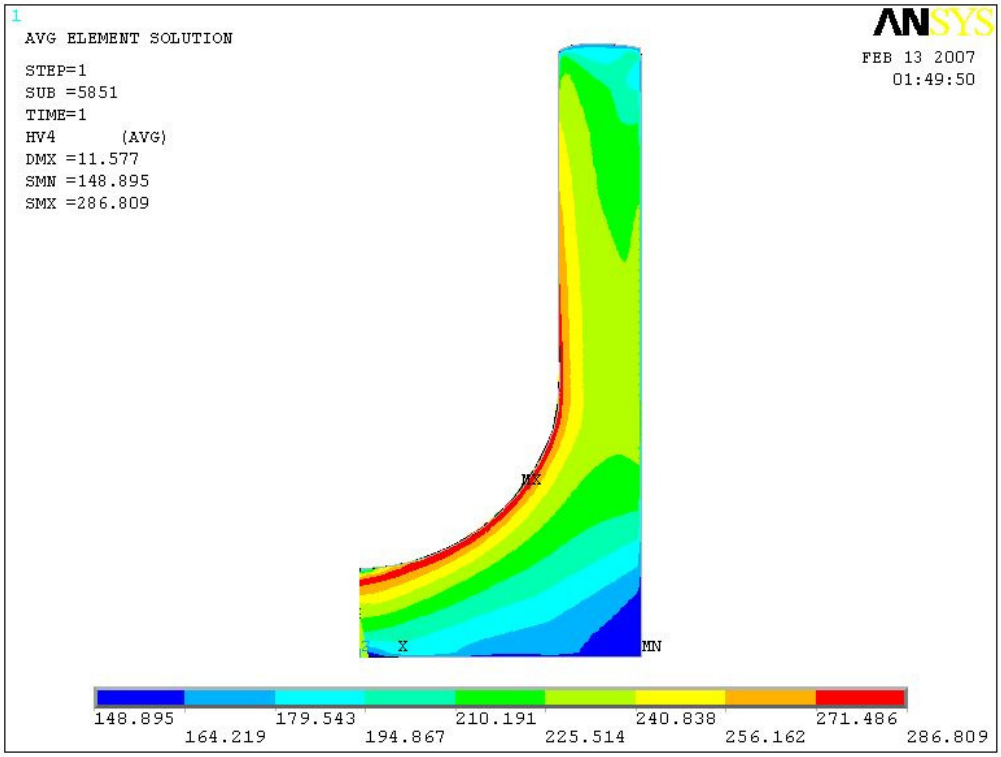

Figure 5.3. The worst Vickers hardness distribution

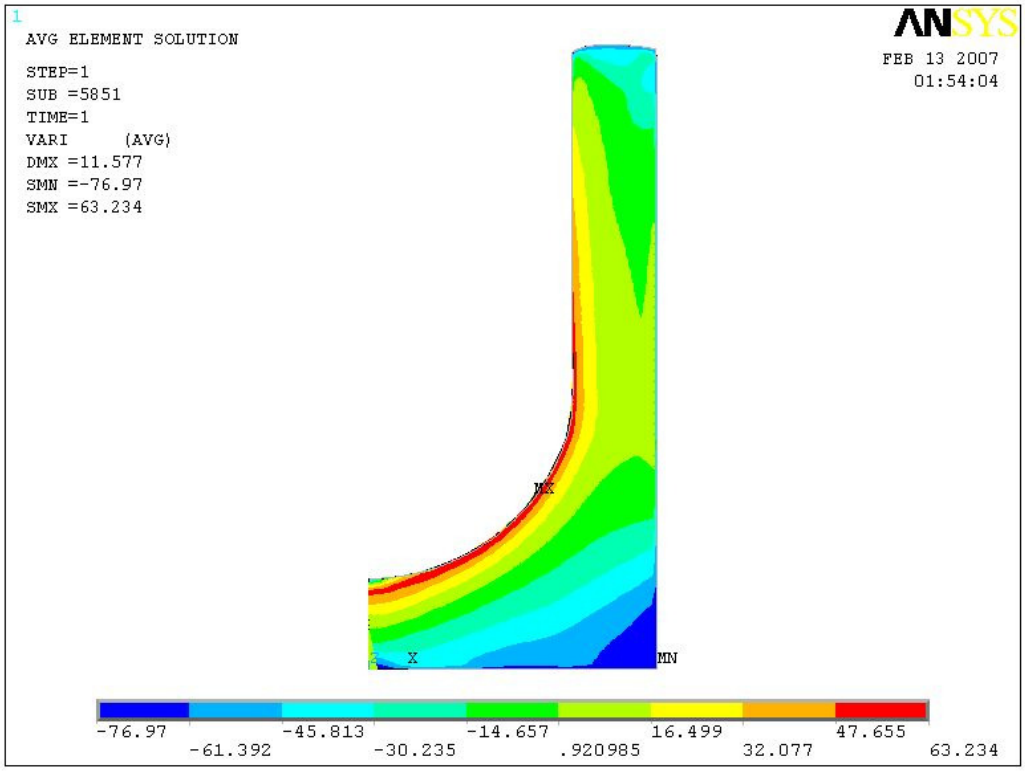

Figure 5.4. The variation in Vickers hardness for the worst case

5.4. Assumptions and Discussions

In this study, the following assumptions were made which might detract from the accuracy of results. First of all, material flow curve constants K and n for St37 were assumed to be 773 Mpa and 0.171 respectively. These constants define the deformation behavior of the material. Besides, they are also used in the analytical relationship between Vickers hardness and effective strain. The effects of the experimental errors or the errors due to curve fitting were assumed to be negligibly small on the numerically obtained hardness results.

Secondly, up to 8 per cent errors may occur in the predictions of the analytical Vickers hardness-effective strain relationship given in Eq. 3.10. Use of this analytical relationship stated by Sönmez and Demir [8] improves the flexibility of the approach proposed in this study. Since this relationship (given in Eq. 3.10) is based on two universal (ε_o and c) and two flow curve constants (K and n), one may apply this relationship to

another material after obtaining its flow curve constants. Besides, these constants are available in the literature for a wide range of materials.

The effect of friction factor was high on the results as discussed before. In the optimization runs, the FE model used a constant friction factor *m* equal to 0.1 One should correctly determine *m* in any real application.

The initial billet material was assumed to be homogeneous and fully annealed, thus the initial hardness distribution in the billet was uniform. In addition the change in hardness of deformed workpiece was assumed to be a function of induced effective strain and independent of strain path.

Die and punch surfaces were modeled using rigid lines. In practice, these surfaces deform elastically, but these deformations are negligible compared to large plastic deformation induced in the workpiece. Otherwise, areas representing the die and the punch need to be meshed in order to obtain deformation history of them which highly increases required computational capacity.

In this study, optimization variables are mainly constrained by geometric requirements. One may integrate new constraints and improve effectiveness of the proposed methodology. Forgability of the product may be investigated by observing induced stresses in the material. Then, a constraint may be set for maximum allowable stress above which internal cracks develop in the workpiece. In addition, a set of constraints may be defined to prevent the die and the punch being exposed to stresses higher than their yield strength. The required press power may also be obtained, and that may be used as a constraint related to economic considerations.

6. SUMMARY AND CONCLUSIONS

In this thesis, a methodology was proposed to improve the hardness distribution in a backward extruded cup by optimizing preform and die shapes.

The literature survey showed that the resulting hardness distribution in cold formed parts could be analytically related to the extent of induced plastic strains. Thus, the analytical strain-hardness relation proposed by Sönmez and Demir [8] was adopted in this study to obtain hardness distribution in a backward extruded workpiece made of St37 steel. Since plastic strains induced in cold formed workpieces could not be obtained analytically, a finite element model of the process was developed. Having obtained the hardness distribution in the workpiece and ensured the convergence of results, process optimization was conducted. Two variables defining the punch tip geometry (*R1* and *R2)* and one variable defining the clearance between the die and the workpiece (*t*) were selected as optimization variables. The objective function was expressed as the sum of variations from the average hardness. The ranges of values that optimization variables could take were constrained because of the limitations related to the process, product requirements and finite element analysis. Penalty functions were utilized in order to account for constraint violations. Nelder-Mead was selected as the search algorithm since it is a robust zero order algorithm which makes decisions based on the values of the objective function and does not require the calculation of any derivatives. An optimization code was developed using ANSYS Parametric Design Language incorporating the finite element model and the optimization procedure.

The optimum values for the optimization variables *R1*, *R2* and *t*, were obtained as 31.5, 2.0 and 0.01 mm respectively. The minimized (best) objective function value was 9.573, and the maximum (worst) objective function value was 18.007, which refers to a possible improvement of 46.8 per cent in the objective function in comparison to that of an arbitrarily chosen design parameters.

In addition to the achieved improvements in the hardness distribution, two important design guidelines for an improved hardness distribution were suggested based on the

outputs of the optimization procedure. Firstly, the lower the clearance between the die walls and the preform, the smaller the variation in the hardness distribution. Secondly, more effective lubrication results in a more homogeneous hardness distribution. In other words, there is a negative correlation between the friction coefficient for the die-workpiece interface and the degree of variation in the hardness distribution.

The methodology proposed in this thesis is applicable to other types of materials as well is to other cold forming processes. If a researcher has the required information about the mechanical properties of the material in concern and developed a reliable FE model of the process in concern, he/she can adopt the proposed methodology in his/her own study. In addition to different geometric optimization variables, different variables and constraints may be defined to enlarge the scope of the proposed method. For instance, stresses developed in the tooling may be constrained to prevent tooling failures or improve tooling life. The propped methodology may also be adapted to multi-stage cold forming processes.

APPENDIX A: DEFINING SPECIFIC OUTPUTS IN ANSYS

Although ANSYS offers a wide variety of output types, researchers may need a specific kind of output which is not a default one. In this case, researchers may define their specific output type if they can relate the required entity and one of the default outputs analytically.

In this study, Vickers hardness is obtained using effective strain which is not a predefined output type in ANSYS. Eq. (3.10) in section 3.1 shows that effective strain is a function of principal strains. In addition, the analytical relation between Vickers hardness and effective strain is given in Eq.8. Using these analytical relationships, one may make ANSYS give effective strain and hardness output data, and display distribution of them as contour plots (Figure.4.9 and 4.13). Specific analysis results are obtained in two different ways. The first way is to define required entities as scalar or array parameters. The other way is to use element tables, which is a must if contour plots are essential.

A.1. Use of Array and Scalar Parameters

Use of array or scalar parameters is advantageous if required output data are stored in text format. Parameters may be used in any kind of mathematical operations. They can be written in output files, and ANSYS is able to read parameter values from input files.

The method to obtain Vickers hardness at selected nodes using scalar and array parameters is explained below. Further details of used commands are given in the related ANSYS help files.

As mentioned before, the first step of obtaining the required output type is to determine the default source data. In section 3.1, the strain-hardness relation briefly explained. Therefore; first, second and third principal strains at all nodes in the area representing the workpiece should be obtained.

The code given below is taken from the optimization code created in this study. The total number of nodes is expressed by *MxNr* being a scalar parameter. *HVArry* is the name of the array consisting of (1 X *MxNr*) parameters. The index of do-loop is *i*. The first, second and third principal strains are expressed as *PrStr1*, *PrStr2* and *PrStr3* respectively. *EffStr* represents effective strain of the selected node. *HV* represents Vickers hardness of ith node. *HVArry(i)* relates the position of *i*th *HV* in *HVArry*. Note that line numbers (L1, L2, ..., LN) are only valid for explanations and omitted in command files.

```
L1    *DIM, HVArry, ARRAY, MxNr
L2    *DO, i,1, MxNr
L3    *GET, PrStr1, NODE, i, EPPL, 1
L4    *GET, PrStr2, NODE, i, EPPL, 2
L5    *GET, PrStr2, NODE, i, EPPL, 1
L6    EffStr=SQRT (2/3*(PrStr1**2+ PrStr2**2+ PrStr3**2))
L7    HV=0.10197*2.9*773*(0.08+EffStr)**0.171
L8    HVArry(i)=HV
L9    *ENDDO
```

L1) Creates a 1D array (1 X *MxNr*)

L2) Starts a loop with index *i* from 1 to *MxNr*

L3) Reads fist principal strain of selected node, and appoints it to the scalar parameter *PrStr1*

L4) Reads second principal strain of selected node and appoints it to scalar parameter *PrStr2*

L5) Reads third principal strain of selected node and appoints it to scalar parameter *PrStr3*

L6) Calculates effective strain of selected node and appoints it to the scalar parameter *EffStr*

L7) Calculates Vickers hardness of selected node and appoints it to scalar parameter *HV*

L8) *HV* is stored as the *i*th parameter of *HVArry(i)*

L9) Terminates the loop

Array parameter *HVArry* may be used for further calculation or written in a text file. To create a text file and write parameters in it, following codes are used.

```
L1      *CFOPEN, VH, TXT
L2      *DO, i, 1, MxNr
L3      /OUTPUT, VH, TXT, APPEND
L4      *VWRITE, i, 'HV=', HVArry(i)
L5      (F10.0, A9, F10.3)
L6      /OUTPUT
L7      *CFCLOSE
L8      *ENDDO
```

L1) Opens a text file labeled *VH.txt*

L2) Starts a loop to write all parameter values of *HVArry*, where *i* is the loop index.

L3) Directs the text output to the previously created file, *VH.txt*

L4) Indicates data to be written in the output file.

L5) Determines writing format (same as the fortran display format).

L6) Redirects output to the screen

L7) Closes the text file.

L8) Terminates the loop.

The first three lines of the resulting text file are given below.

```
1.  HV=   210.234
2.  HV=   222.336
3.  HV=   234.560
```

A.2 Use of Element Tables

Scalar or array parameters can only be used by keyboard entries or making ANSYS read a text file including required commands. In contrast, element tables can be created either using GUI or creating command files.

Element tables can be defined and operated easily by using command files. Below is given the codes to obtain Vickers hardness distribution plot, starting from principal strains. See analytical relations given in section 2.1. Hardness-Strain Relations to validate given command lines.

```
L1    /POST1
L2    AVPRIN, 0, ,
L3    ETABLE, Pstr1, EPPL,1
L4    AVPRIN, 0, ,
L5    ETABLE, Pstr2, EPPL,2
L6    AVPRIN, 0, ,
L7    ETABLE, Pstr3, EPPL,3
L8    SEXP, Sq1, Pstr1, , 2,1,
L9    SEXP, Sq2, Pstr2, , 2,1,
L10   SEXP, Sq3, Pstr3, , 2,1,
L11   SADD, Ad1, SQ1, SQ2,1,1, ,
L12   SADD, Ad2, Ad1, SQ3, 1,1, ,
L13   SMULT, Multip, Ad2, , 0.66666,1,
L14   SEXP, Efstr, Multip, ,0.5,1,
L15   SADD, Efstr2, Efstr, ,1,0,0.08,
L16   SEXP, HV1, Efstr2, ,0.171,1,
L17   SMULT, HV2, HV1, ,773,1,
L18   SMULT, HV3, HV2, ,2.9,1,
L19   SMULT, HV4, HV3, ,0.10197,1,
L20   PLETAB, HV4, AVG
```

L1) Activates postprocessor

L2) Element table values are calculated as average nodal values

L3) *Pstr1* is defined an element table, including first principal strains

L4) Same as L2

L5) *Pstr2* is defined an element table, including second principal strains

L6) Same as L2

L7) *Pstr3* is defined an element table, including third principal strains

L8) Element table *Sq1 = Prstr1***2, where SEXP is exponential operator

L9) Element table *Sq2 = Prstr2***2

L10) Element table *Sq3 = Prstr3***2

L11) Element table *Ad1=Sq1+Sq2*, where SADD is addition operator

L12) Element table *Ad2=Ad1+Sq3*,

L13) Element table *Multip*=0.66666**Ad2*=2/3**Ad2*, where SMULT is multiplication operator

L14) Element table *Efstr* including effective strain data. *EfStr*=*Mulitp***0.5

L15) Element table *Efstr2*=*Efstr*+0.08

L16) Element table *HV1*= *EfStr2***0.171

L17) Element table *HV2*= *HV1**773

L18) Element table *HV3*= *HV2**2.9

L19) Element table *HV4*= *HV3**0.10197

L20) Plots *HV4* using nodal average values of elements

In the Section 4, effective strain and Vickers Hardness distribution are plotted using element tables. To define element tables, use the path in GUI main/general postproc/elemet table/define table. In the following screen click "Add" .In the next screen, enter the name of the element table to be created (1 in Figure A.1). Select desired type of output (2 and 3). Click "Apply" to define a new element table or click "Ok" to exit (4). This operation creates an element table including first principal strains and named *Prstr1*. Same operation are to be repeated in order to define *Prstr2 and Prstr3*.

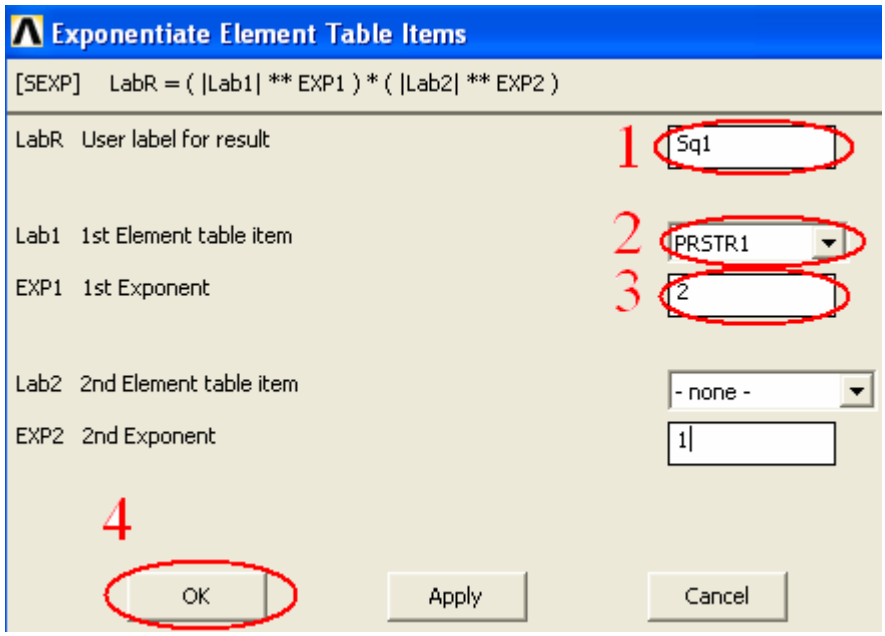

Figure A.1. Definition of element tables in GUI

As mentioned above, arithmetical operations should be applied on element tables. Figure A.2 shows, how to define analytical relation *Sq1=Prstr1***2. First follow the path in GUI main/general postproc/elemet table/exponentiate. In the following screen, enter the name of the resulting element (1). Select the previously created element table *Prstr1*(2). Then, enter the exponent (3). Click "Apply" to define a new operation or click "Ok" to exit (4).

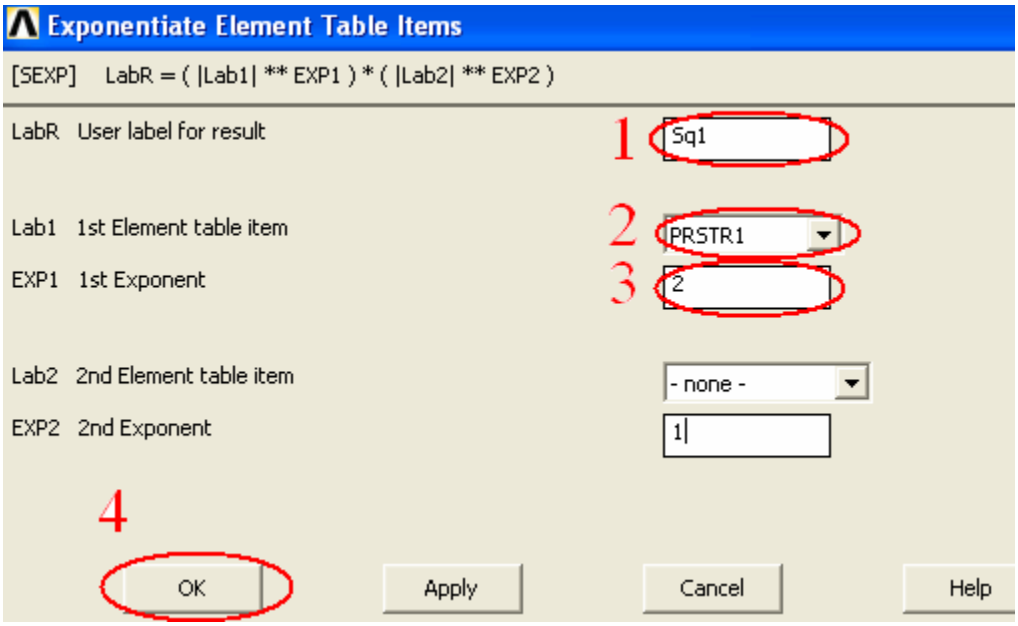

Figure A.2. Exponentiation of *Prstr1*

To plot desired element table follow the path in GUI main/general postproc/elemet table/plot elem table or main/general postproc/plot results/contour plot/ elem table. Select one of the previously defined element tables (1 in Figure A.3). Select "yes, average" option for plots with averaged nodal values (2). Click "OK" to exit.

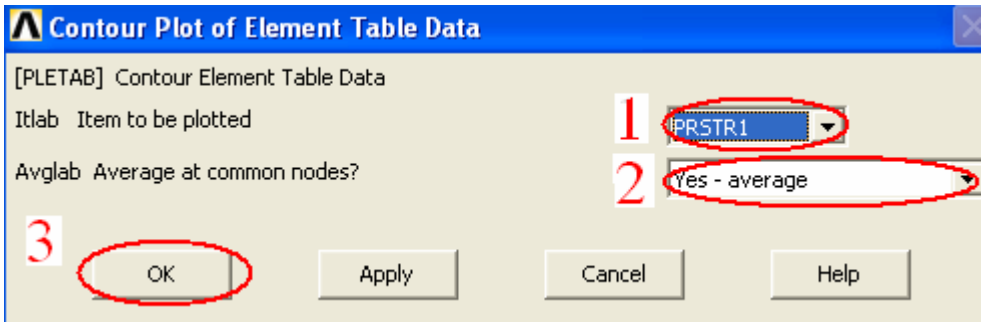

Figure A.3. Settings for element table plot of first principal strain

APPENDIX B: HARDNESS CONVERSION

Hardness scales can be converted into each other using conversion charts and tables. A sample chart is given in Figure B.1 which is created for conversion of Vickers hardness to different Rockwell hardness scales for hard materials.

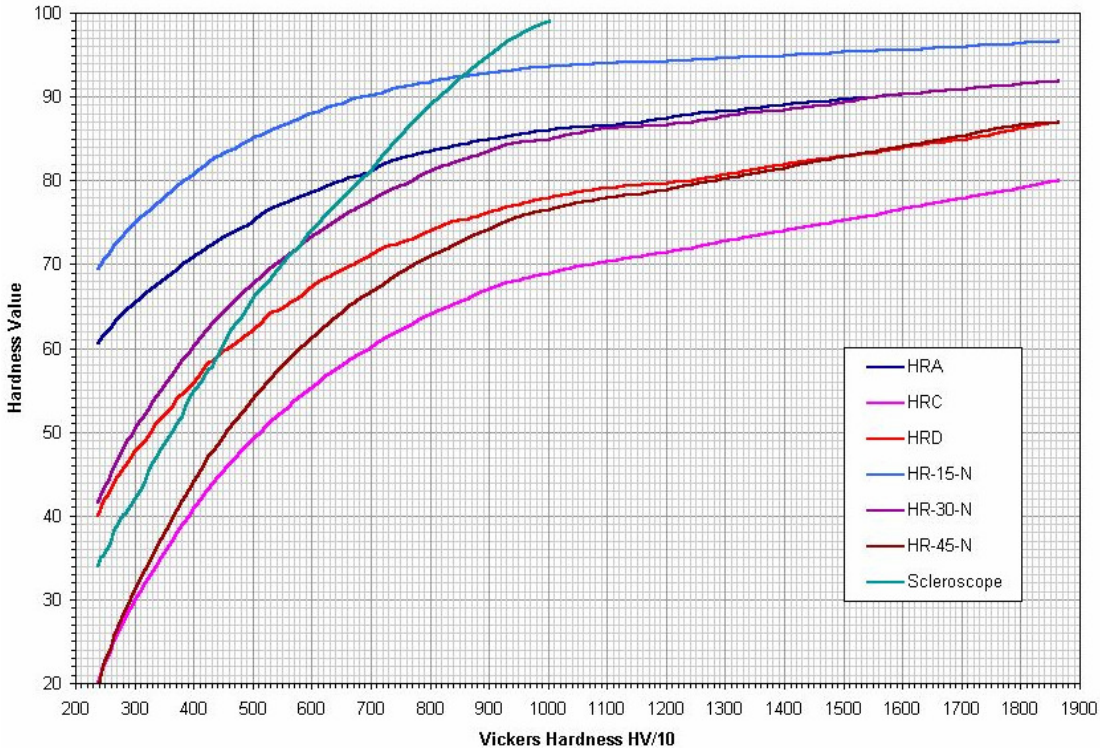

Figure B.1. Hardness conversion chart HV to HR for hard materials [17]

Below is given a conversion table for carbon and alloy steels. In Figure 4.12, Vickers Hardness distribution of backward extruded specimen is plotted. Note in this plot that hardness changes between 150 and 290 HV. Although hardness conversion between different methods and scales cannot be made mathematically exact for a wide range of materials, a linear approximation between 131 and 311 HV is made using data obtained from Table B.1.. Data points selected for this approximation are given in Table B.2. Figure B.2 shows Vickers vs. Brinell hardness plot and the linear approximation curve. The equation of this linear approximation curve is given in Eq.B.1. Using this equation, HV is converted to Brinell Hardness (HB) scale.

$$HB = 1.0593 \cdot HV - 1.6666 \quad \text{(B.1)}$$

Table B.1. Approximate equivalent hardness number and ultimate tensile strengths for carbon and alloy steels [18]

		Rockwell		Ultimate	σu
Brinell HB	**Vickers HV**	**HRB**	**HRC**	**Mpa**	**ksi**
627	667	-	58.7	2393	347
578	615	-	56.0	2158	313
534	569	-	53.5	1986	288
495	528	-	51.0	1813	263
461	491	-	48.5	1669	242
429	455	-	45.7	1517	220
401	425	-	43.1	1393	202
375	396	-	40.4	1267	184
341	360	-	36.6	1131	164
311	328	-	33.1	1027	149
277	292	-	28.8	924	134
241	253	100	22.8	800	116
217	228	96.4	-	724	105
197	207	92.8	-	655	95
179	188	89.0	-	600	87
159	167	83.9	-	538	78
143	150	78.6	-	490	71
131	137	74.2	-	448	65
116	122	67.6	-	400	58

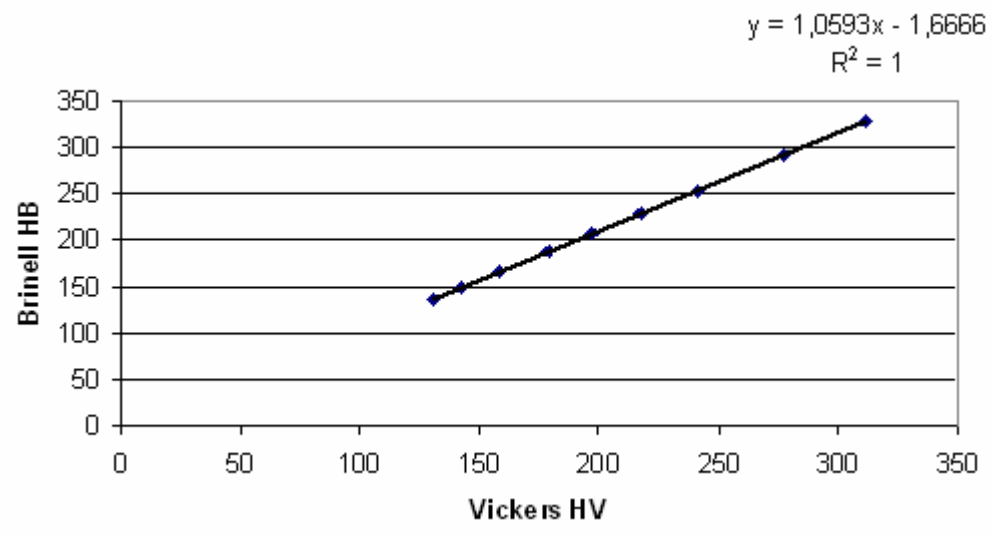

Figure B.2. HV-HB relation between 131-311 HV

Table B.2. Selected data for linear approximation

	HB	HV
1	137	131
2	150	143
3	167	159
4	188	179
5	207	197
6	228	217
7	253	241
8	292	277
9	328	311

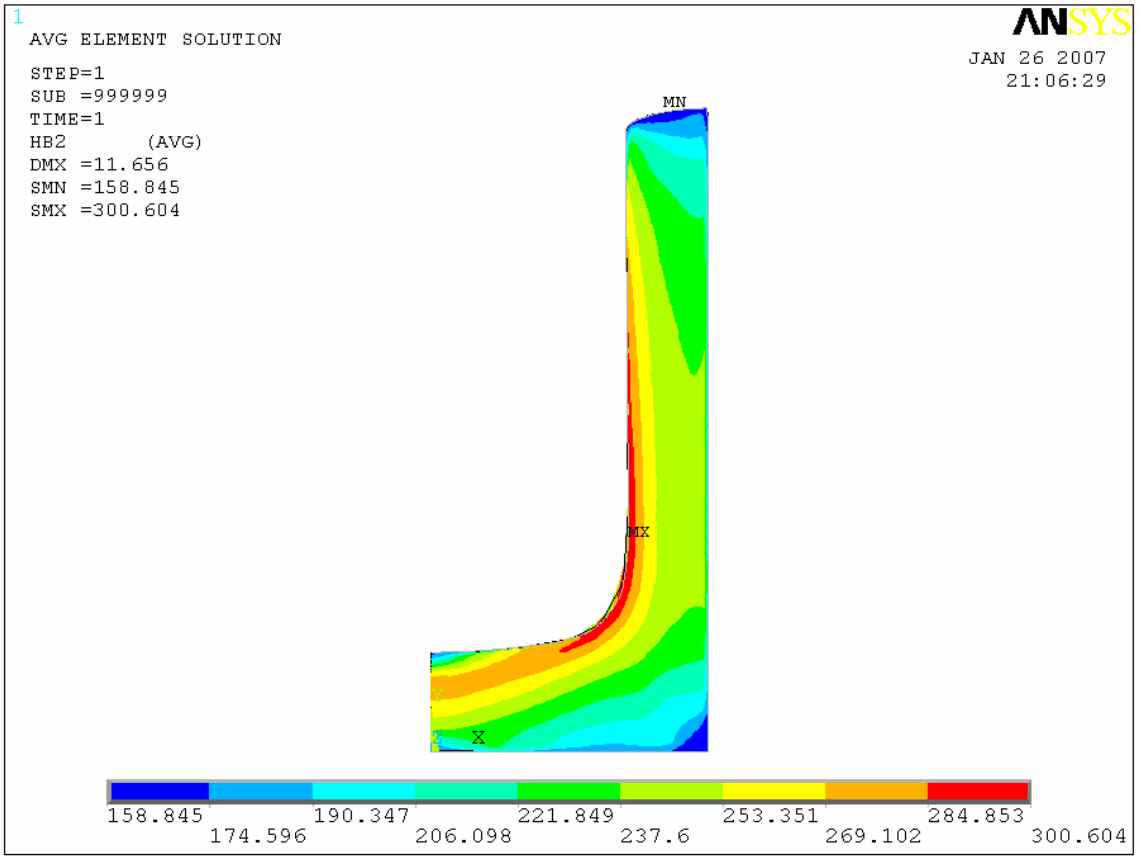

Figure B.3. Brinell hardness distribution plot converted from Figure 4.12

APPENDIX C: FLOW CURVE DATA USED IN MISO MODEL

Table C.1. Flow curve Data used in MISO Model

K		**n**	**ST 37**		
773		0.171			
Nr	**ε**	**σ**	**Nr**	**ε**	**σ**
1	0	0	**20**	0.500	686.6
2	0.001	244.1	**21**	0.550	697.9
3	0.002	267.1	**22**	0.600	708.3
4	0.003	286.3	**23**	0.700	727.3
5	0.004	300.7	**24**	0.800	744.1
6	0.005	312.4	**25**	0.900	759.2
7	0.025	411.4	**26**	1.000	773.0
8	0.060	477.8	**27**	1.250	803.1
9	0.100	521.4	**28**	1.500	828.5
10	0.150	558.8	**29**	1.750	850.6
11	0.200	587.0	**30**	2.000	870.3
12	0.250	609.9	**31**	2.250	888.0
13	0.275	619.9	**32**	2.500	904.1
14	0.300	629.2	**33**	2.750	919.0
15	0.325	637.8	**34**	3.000	932.8
16	0.350	646.0	**35**	3.250	945.6
17	0.375	653.6	**36**	3.500	957.7
18	0.400	660.9	**37**	3.750	969.0
19	0.450	674.3	**38**	4.000	979.8

APPENDIX D: THE NELDER - MEAD METHOD

The Nelder Mead Method is a robust zero order search algorithm not requiring numerical derivatives of the objective function. The method uses a simplex, which is a polytope of n+1vertices in n dimensions. For one variable, the simplex is a line segment. For two variables, the simplex is a triangle, and it becomes a tetrahedron (Figure D.1) for cases with three optimization variables.

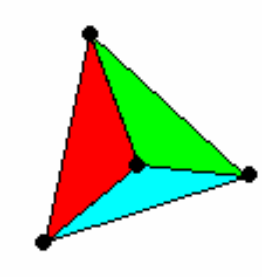

Figure D.1. The simplex as a tetrahedron for three variables

Basically, the method is a pattern search that compares function values at vertices. The worst vertex, where the function value becomes largest, is rejected and replaced with a new vertex. A new simplex is formed and the search is continued. The process generates a sequence of simplex for which the function values at the vertices get smaller and smaller. Finally, the size of the simplex is reduced and the coordinates of the minimum point are found (Figure D.2).

The Nelder - Mead Algorithm is easier to explain for cases with two optimization variables, where the simplex is a triangle in 2D. Below is given the logical decisions made in Nelder Algorithm and short explanations of used terms. In this study, the Nelder-Mead algorithm is applied for three optimization variables resulting in four vertices. The differences between the two and three variable cases are also given below which is rarely depicted in text books.

The method requires the calculation of the objective function at three initial vertices. Then, the vertices are ordered from the smallest to greatest and denoted as B (best), G

(good) and *W* (worst), respectively. For three optimization variables, initial vertices are denoted as *B* (best), *G* (good), *V* (worse) and *W* (worst).

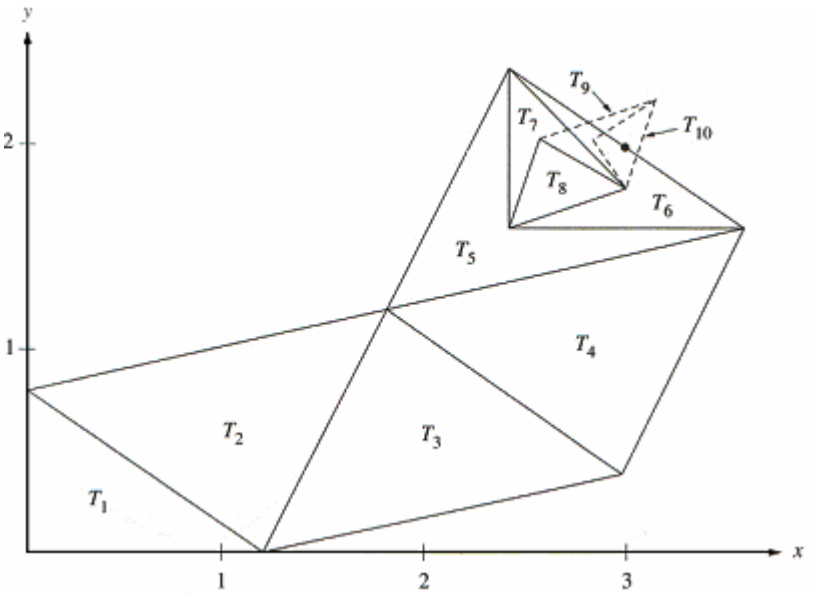

Figure D.2. The sequence of triangles converging to the minimum point [16]

The method requires the calculation of the objective function at three initial vertices. Then, the vertices are ordered from the smallest to greatest and denoted as *B* (best), *G* (good) and *W* (worst), respectively. For three optimization variables, initial vertices are denoted as *B* (best), *G* (good), *V* (worse) and *W* (worst).

The midpoint *M* is the point in the middle of line segment joining *B* and *G* vertices of triangle and calculated by Eq. D.1.

$$\vec{M} = \vec{B} + \vec{G} = \left(\frac{x_M + x_G}{2}, \frac{y_M + y_G}{2} \right) \tag{D.1}$$

For tetrahedron the midpoint *M* is found by Eq. D.2.

$$\vec{M} = \vec{B} + \vec{G} + \vec{V} = \left(\frac{x_M + x_G + x_V}{3}, \frac{y_M + y_G + y_V}{3}, \frac{z_M + z_G + z_V}{3} \right) \tag{D.2}$$

It is likely that the function takes smaller values away from *W* on the opposite side of the line *AB*. The behavior of the function on this side is checked on the reflection point *R*, which is obtained using Eq. D.3. Midpoint *M* and reflection point *R* are shown in Figure D.3 for triangular simplex and in Figure D.4 for tetrahedronal simplex.

$$\vec{R} = M + \left(\vec{M} - \vec{W}\right) \tag{D.3}$$

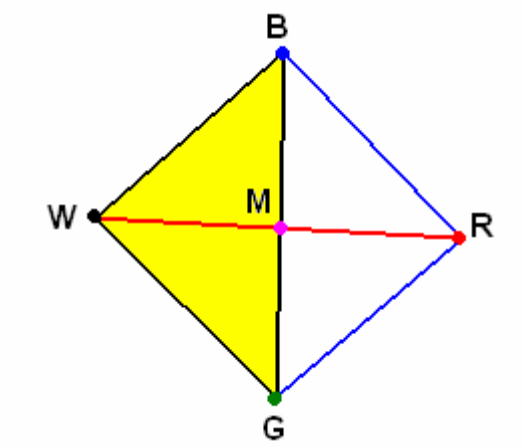

Figure D.3. Midpoint and reflection point for triangle

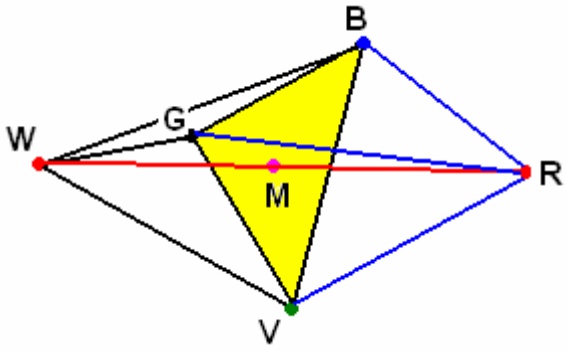

Figure D.4. Midpoint and reflection point for tetrahedron

If the reflection point yields a smaller function value, then it is extended to find a possibly better point lying further than the point *R*. Thus, the expansion point *E* is calculated (Eq. D.4). If *E* is a better point than *B*, then *W* is replaced by *R*, otherwise *W* is replaced by *R*. The equation giving expansion point is the same for triangular and tetrahedron simplex. Figure D.5 and Figure D.6 describe expansion of the simplex.

$$E = \vec{R} + \left(\vec{R} - \vec{M}\right) \tag{D.4}$$

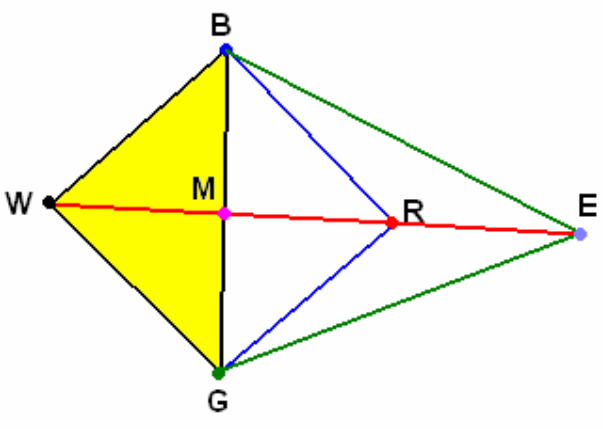

Figure D.5. Expansion using *R* in 2D

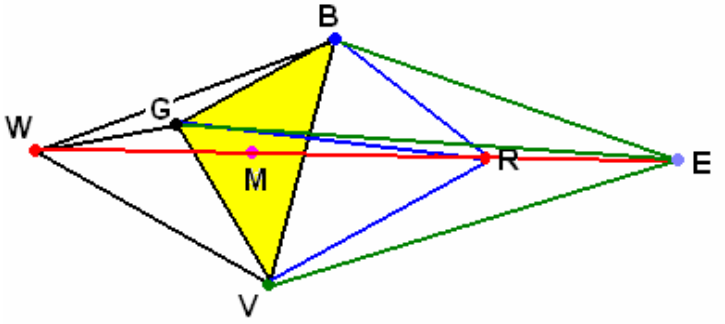

Figure D.6. Expansion using *R* in 3D

$$\vec{C} = \frac{\vec{W} + \vec{M}}{2} \tag{D.5}$$

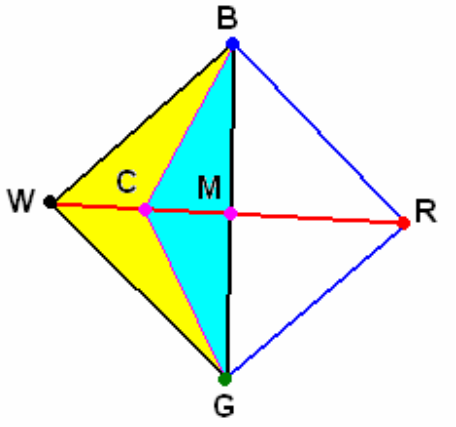

Figure D.7. New contracted triangle *BCG*

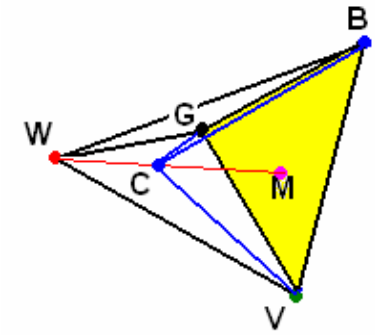

Figure D.8. Contraction of tetrahedron by *C*

If the objective function having a greater value at *C* compared to *W,* the triangle should be shrunk toward *B*. The resulting triangle is *BSM*. S is calculated by Eq. D.6. For tetrahedron, three shrink points are required, which are obtained by Eq. D.7, Eq. D.8 and Eq. D.9.

$$\vec{S} = \frac{\vec{B} + \vec{W}}{2} \tag{D.6}$$

$$\vec{S}_1 = \frac{\vec{B} + \vec{G}}{2} \tag{D.7}$$

$$\vec{S}_2 = \frac{\vec{B} + \vec{V}}{2} \tag{D.8}$$

$$\vec{S}_3 = \frac{\vec{B} + \vec{W}}{2} \tag{D.9}$$

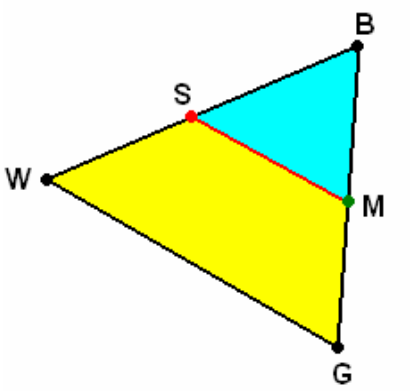

Figure D.9. Shrink toward *B*

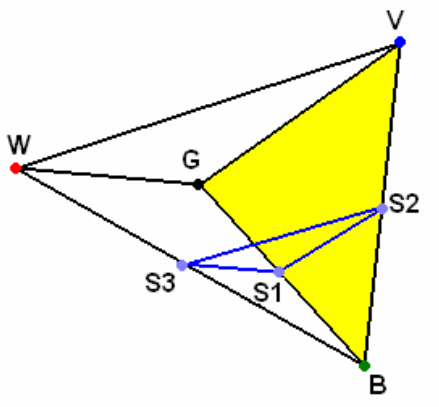

Figure D.10. Shrinking tetrahedron by S1, S2 and S2

Shrinkage of triangle and tetrahedron toward B are shown in Figure D. 9 and Figure D.10.

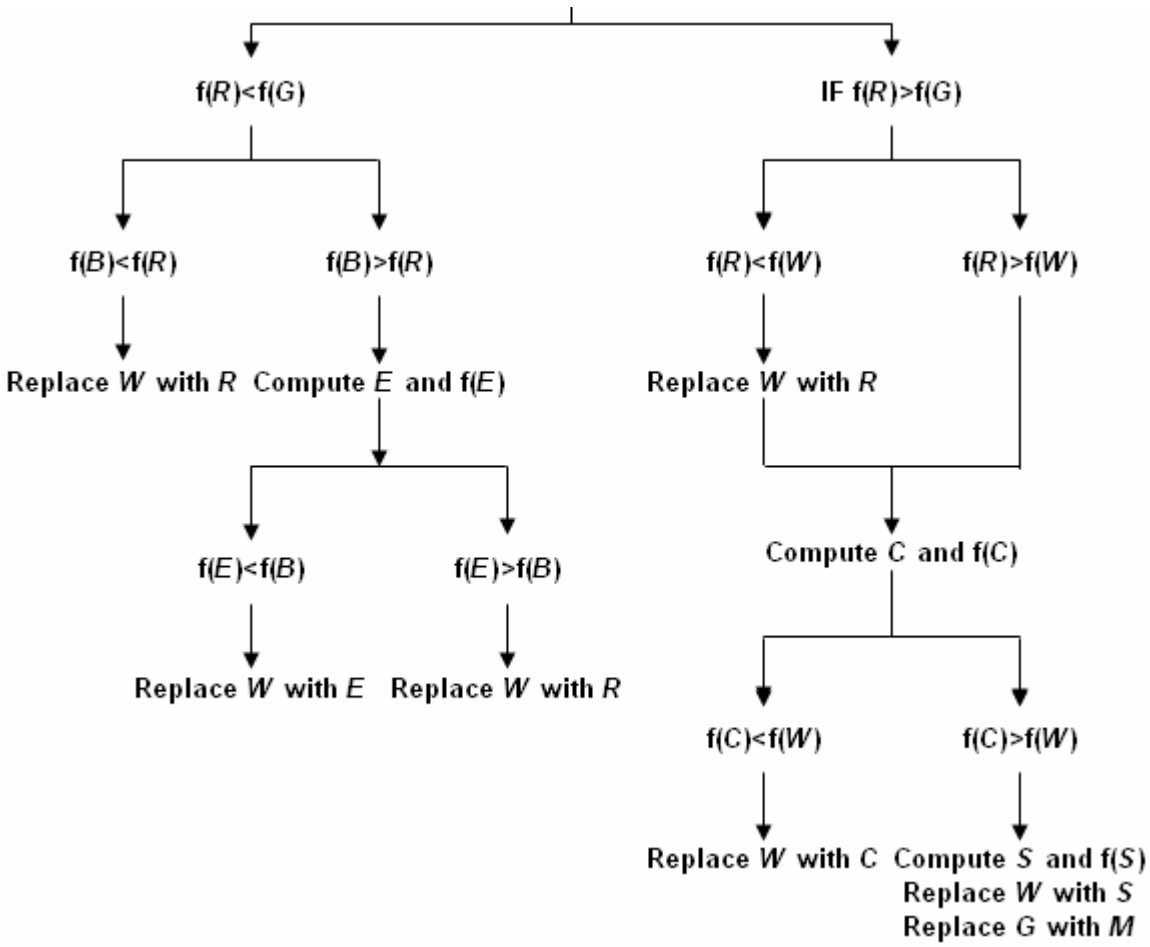

Figure D.11. Logical decisions for the Nelder-Mead algorithm

Process steps of the Nelder-Mead algorithm are given in Figure D.11. Following these steps and using equations given above, optimum points are obtained. Note that the Nelder-Mead algorithm gives the local minimum. In order to obtain the global minimum, optimization procedure needs to be repeated with different initial vertices

REFERENCES

1. Altan, T., G. Ngaile and G. Shen, *Cold and Hot Forging- Fundamentals and Applications*, ASM International, Ohio, 2005.

2. Thiyagarajan, N. and R. V. Grandhi, *Multilevel Design Process for 3D Preform Shape Optimization in Metal Forming*, Journal of Materials Processing Technology, Vol. 170, pp. 421-429, 2005.

3. Zhao, X., G. Zhao, G. Wang and T. Wang, *Preform Die Shape Design for Uniformity of Deformation in Forging Based on Preform Sensitivity Analysis*, Journal of Material Processing Technology, Vol. 128, pp.25-32, 2002.

4. Shi, X., J. Chen, Y. Peng and X. Ruan, *A New Approach of Die Shape Optimization for Sheet Metal Forming Processes*, Journal of Material Processing Technology, Vol. 152, pp. 35-42, 2004.

5. Celano, G., S. Fichera, L. Fratini and F. Micari, *Application of AI Techniques for the Optimal Design of Multipass Cold Drawing Processes*, Journal of Material Processing Technology, Vol. 113, pp. 680-685, 2001.

6. Gao, Z. and R.V. Grandhi, *Microstructure Optimization in Design of Forging Processes, International Journal of Machine Tools and Manufacture*, Vol. 40, pp. 691-711, 2000.

7. Roy, S., S. Ghosh and R. Shivpuri, *A new Approach to Optimal Design of Multi-Stage Metal Forming Processes with Micro Genetic Algorithms*, International Journal of Machine Tools and Manufacture, Vol. 37 (1), pp. 29-44, 1997.

8. Demir, A. and F. Ö. Sönmez, *Prediction of Brinell Hardness Distribution in Cold Formed Parts*, Journal of Materials Processing Technology, Vol. 126, pp. 398-405, 2004.

9. Hur, K. D., Y. Choi and H. T. Yeo, *A Design Method for Cold Forward Extrusion using FE Analysis*, Finite Elements in Analysis and Design, Vol. 40, pp. 173-185, 2003.

10. Kim, H., S-M Lee and T. Altan, *Prediction of Hardness Distribution in Cold Backward Extruded Cups*, Journal of Materials Processing Technology, Vol. 59, 113-121, 1996.

11. Petruska, J., L. Janicek, *On the Evaluation of Strain Inhomogeneity by Hardness Measurement of Formed Products,* Journal of Materials Processing Technology, Vol. 143-144, pp. 300-305, 2003.

12. Tabor, D., *A Simple Theory of Static and Dynamic Hardness*, Proceedings of the Royal Society of London, Series A, Mathematical and Physical Sciences, Vol. 192, Issue 1029, pp. 247-274, 1948.

13. Gonzales, F. U., *A discussion on Modern Design Optimization Tools: Full Associativity of CAD, FEA and Event Simulators*, http://www.algor.com/news_pub /tech_white_papers/design_optimization/default.asp, 2006.

14. Ansys, *Release 10.0 Documentation*, ANSYS Inc., 2005.

15. Gouveia, B.P.P.A., J.M.C. Rodrigues, N. Bay and P. A. F. Martins, *Finite Element Modeling of Cold Forward Extrusion*, Journal of Materials Processing Technology Vol. 94, pp.85-93, 1999.

16. Mathews, H. and K. D. Fink, *Numerical Methods Using Matlab-Third Edition*, Prentice Hall Inc., New Jersey, 1999.

17. England, G., *Hardness Conversion Chart for Hard Materials (Rockwell C Range)*, http:// www.gordonengland.co.uk/hardness/rockwell_c_conv.htm, 2007.

18. Dowling, N. E. , *Mechanical Behavior of Materials-Second Edition*, Prentice Hall Inc., New Jersey, 1999.